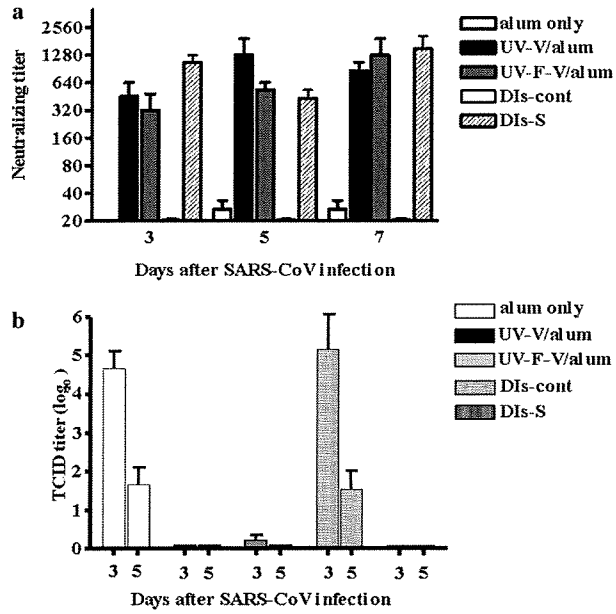

Fig. 3. (a) Neutralizing titers in the plasma of vaccinated mice. Titers were calculated as previously described (15). (b) SARS-CoV titers in the lung lavage of vaccinated mice. Bar shows the SEM ($n = 3$).

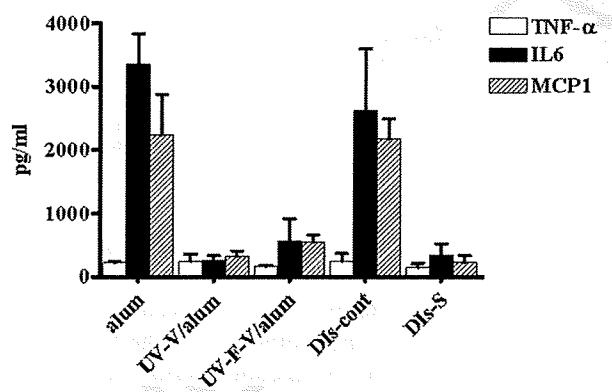

Fig. 4. Concentrations of TNF-α, IL-6 and MCP-1 in the lung lavage of vaccinated mice. Cytokines and chemokines in the lung lavage of vaccinated and control mice on day 3 after SARS-CoV infection were assayed by flow cytometry using a mouse inflammatory cytokine (IL-6, IL-10, MCP-1, IFN-γ, TNF-α and IL-12p70) cytometric bead array kit. Bar shows the SEM ($n = 3$).

epitope of SKOT-20 localizes to the RBD of the S protein and exhibits the most potent neutralizing activity (18). To demonstrate that the anti-spike neutralizing antibody is mainly responsible for the protective efficacy we observed in SARS model mice, we administered SKOT-20 i.p. once, just before Pp infection. As shown in Figure 5a, the mice treated with SKOT-20 recovered from the loss of bodyweight and were resistant to the fatal outcome as we observed in vaccinated mice.

When we measured a virus titer in the lung lavage at day 3 after SARS-CoV infection, it was dramatically decreased in accordance with the concentration of neutralizing antibody given (Fig. 5b). The level of serum neutralizing antibody in these mice was proportionally high at this time point. The neutralizing activity was low but still detectable in the lung lavage. These results clearly show that the neutralizing antibody against S protein is highly effective to prevent SARS development.

Kinetics of cytokine and chemokine production

We have observed a high level of IL-6 and MCP-1 production in Pp and SARS-CoV-coinfected mouse lung lavage at day 3 after SARS-CoV infection (Fig. 4). However, the cytokine profiles in these mice may be variably modified by Pp infection alone, SARS-CoV infection, or both. Therefore, we measured 20 cytokines in lung lavages of these protected and unprotected mice by using a mouse cytokine 20-plex antibody bead kit at day 0 (after Pp infection before SARS-CoV infection), day 1, day 2 and day 3 after SARS-CoV infection as previously reported (16). The production of two cytokines, IL-6 and MCP-1, were increased at days 2 and 3 after SARS-CoV infection in association with high titers of SARS-CoV, as shown in Figure 4. Interestingly, the production of IL-6 was increased by Pp infection alone, decreasing on day 1 and increasing again, whereas that of MCP-1 increased only after SARS-CoV infection. These cytokines were not increased in protected mice (Fig. 6a), suggesting the importance of these two cytokines in the lung pathogenesis. Other cytokine profiles are shown in Figure 6b and c. The level of IP-10 was quite high after SARS-CoV infection on day 1. However, even protected mice produced a high level of IP-10. In contrast, macrophage inflammatory protein (MIP)-1α, TNF-α, and KC were produced only before SARS-CoV infection and the levels of IFN-γ and VEGF were consistently low. The concentrations of other cytokines were low or below the limit of detection (data not shown). These results suggest that IL-6 and MCP-1 play some roles in the lung pathogenicity by Pp and SARS-CoV coinfection.

DISCUSSION

In the present study, we evaluated the protective efficacy of our SARS vaccine candidates: UV- or UV-plus-formalin-inactivated whole virion and recombinant DIs expressing the S protein (DIs-S) using a murine model system of severe respiratory disease caused by the coinfection of Pp and SARS-CoV. The results shown in this paper suggest that whole virion vaccines, either with or without formalin treatment, and DIs-S were protective against a

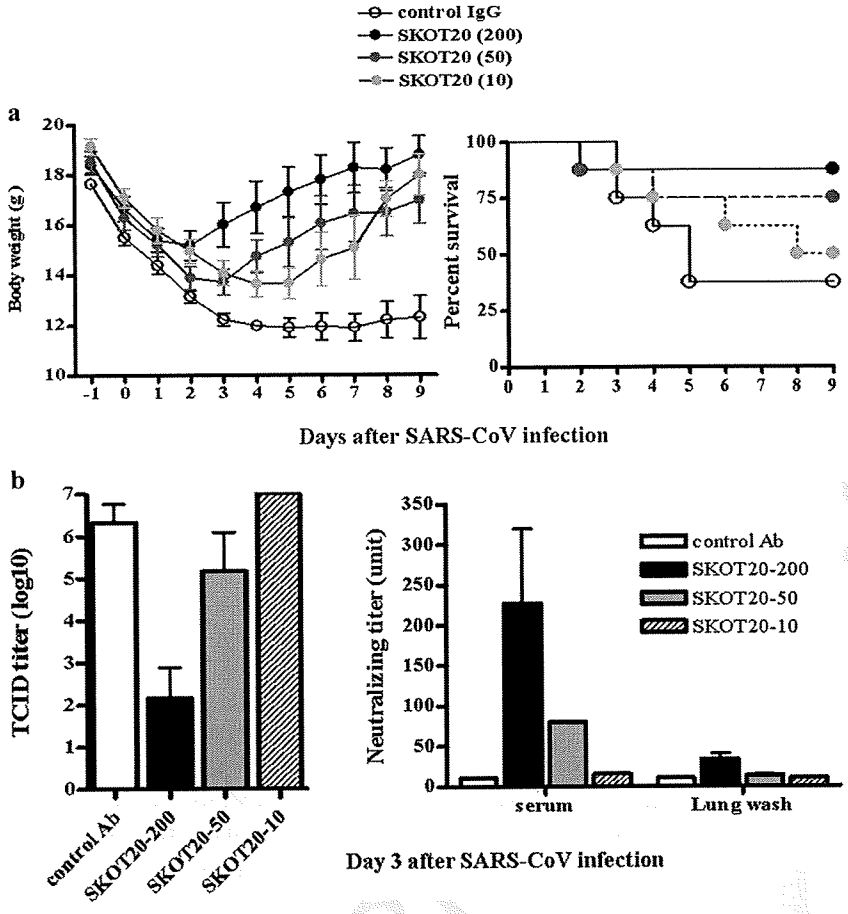

Fig. 5. (a) (Left) Bodyweights of mice injected with SKOT-20 in a murine model system of severe respiratory disease caused by the coinfection of Pp and SARS-CoV. Mice were i.p. injected with 10, 50 or 200 μg SCOT-20 just before Pp infection and weighed daily. Mice were injected with 10 μg (◉), 50 μg (◉), or 200 μg (●) of SKOT-20 or 200 μg control IgG (○). Bar shows the SEM ($n > 8$). (Right) Survival curves of mice injected with SKOT-20. (b) (Left) SARS-CoV titers in the lung lavage of mice injected with SKOT-20. (Right) Neutralizing titers in serum and lung lavage of mice injected with SKOT-20. Bar shows the SEM ($n = 3$).

highly pathogenic pulmonary infection of SARS-CoV in the presence of opportunistic infection by Pp. By giving SKOT-20 just before SARS-CoV infection, the mortality of mice coinfected with Pp and SARS-CoV was dramatically reduced. The level of serum neutralizing antibody in these mice was proportionally high and a virus titer in the lung lavage after SARS-CoV infection was substantially decreased in accordance with the concentration of neutralizing antibody given. Therefore, if a high titer of neutralizing IgG antibody against the S protein is systemically elicited by vaccination, it would be sufficient to prevent SARS development.

Treatment with convalescent plasma has been successfully used to treat SARS, suggesting that passive immunity might be a useful approach by which to combat SARS. (19) Subbarao *et al.* have shown that passive transfer of murine neutralizing antibodies can prevent replication of SARS-CoV in the respiratory tract (20). This antibody has been shown to neutralize the virus *in vitro* and to prevent viral replication in a mouse model of SARS-CoV infection. Sui *et al.* have investigated the antiviral activity of a human monoclonal antibody to the S1 protein that blocks receptor association (21), demonstrating the prophylactic effectiveness of this monoclonal antibody *in vivo* using a mouse model of SARS (9). Recently, several humanized monoclonal antibodies against the S protein have been developed for therapeutic application (22, 23). Many of the neutralizing antibodies against SARS-CoV recognize a RBD in S1 of the spike protein, but other N-terminal domains of the S1 and S2 domains also have neutralizing epitopes (8). For the passive immunization to be highly effective, a combination of neutralizing antibodies recognizing several epitopes of the S protein should be designed so that virus escape mutation can be prevented.

The involvement of cytokines in the SARS pathogenesis has been described (24–26). When the levels of various cytokines and chemokines in the lungs of mice infected with Pp and SARS-CoV were measured, high levels of only IP-10 and IFN-γ production were noted on day 2 following coinfection, but not on day 4 (11). Therefore, the involvement of these cytokines in the high pathogenesis caused by a coinfection with Pp and SARS CoV has been suggested. In this study, we observed that the production of IL-6 and MCP-1 were increased at day 3

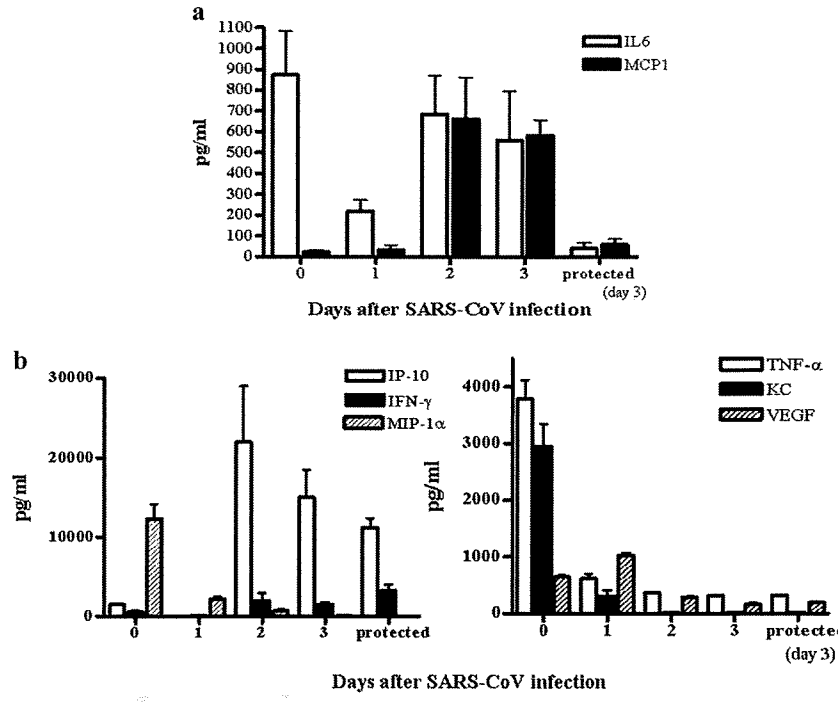

Fig. 6. (a) Concentrations of IL-6 and MCP-1 in the lung lavage of mice infected with SARS-CoV. (b) (Left) Concentrations of IP-10, IFN-γ, and MIP-1α in the lung lavage of mice infected with SARS-CoV. (Right) Concentrations of TNF-α, KC, and VEGF in the lung lavage of mice infected with SARS-CoV. 'Protected' represents the mice injected with 200 μg SKOT-20 before infection with SARS-CoV. Bar shows the SEM ($n = 3$).

after SARS-CoV infection in association with high titers of SARS-CoV, whereas these cytokines were not increased in vaccine-protected mice. Therefore, we analyzed the kinetics of multiple cytokine and chemokine production in detail after Pp only and Pp and SARS-CoV coinfection in naïve and vaccinated mice. Although several cytokines and chemokines were ubiquitously and temporarily upregulated during the lung inflammation caused by these microbes, we found that the levels and profiles of IL-6 and MCP-1 production were well matched with the disease severity and protection. The contribution of these inflammatory cytokines to SARS in humans needs to be investigated further.

ACKNOWLEDGMENTS

The authors gratefully acknowledge Mami Matsuda, Mami Sasaki, Sayaka Yoshizaki, Takuya Yamamoto for technical assistance and Tomoko Mizoguchi for secretarial work. This work was partially supported by a grant-in-aid for Scientific Research from the Japan Society for the Promotion of Science and from the Ministry of Health, Labor, and Welfare of Japan; by the Program for Promotion of Fundamental Studies in Health Sciences of the National Institute of Biomedical Innovation (NIBIO); and by the Research on Health Sciences Focusing on Drug Innovation from the Japan Health Sciences Foundation.

REFERENCES

1. Marra M.A., Jones S.J., Astell C.R., Holt R.A., Brooks-Wilson A., Butterfield Y.S. *et al.* (2003) The genome sequence of the SARS-associated coronavirus. *Science* 300:1399–404.
2. Rota P.A., Oberste M.S., Monroe S.S., Nix W.A., Campagnoli R., Icenogle J.P. *et al.* (2003) Characterization of a novel coronavirus associated with severe acute respiratory syndrome. *Science* **300:** 1394–9.
3. Ruan Y.J., Wei C.L., Ee A.L., Vega V.B., Thoreau H., Su S.T. *et al.* (2003) Comparative full-length genome sequence analysis of 14 SARS coronavirus isolates and common mutations associated with putative origins of infection. *Lancet* **361:** 1779–85.
4. Li W., Moore M.J., Vasilieva N., Sui J., Wong S.K., Berne M.A. *et al.* (2003) Angiotensin-converting enzyme 2 is a functional receptor for the SARS coronavirus. *Nature* **426:** 450–4.
5. Babcock G.J., Esshaki D.J., Thomas W.D., Jr., Ambrosino D.M. (2004) Amino acids 270 to 510 of the severe acute respiratory syndrome coronavirus spike protein are required for interaction with receptor. *J Virol* **78:** 4552–60.
6. Bisht H., Roberts A., Vogel L., Bukreyev A., Collins P.L., Murphy B.R. *et al.* (2004) Severe acute respiratory syndrome coronavirus spike protein expressed by attenuated vaccinia virus protectively immunizes mice. *Proc Natl Acad Sci USA* **101:** 6641–6.
7. Traggiai E., Becker S., Subbarao K., Kolesnikova L., Uematsu Y., Gismondo M.R. *et al.* (2004) An efficient method to make human monoclonal antibodies from memory B cells: potent neutralization of SARS coronavirus. *Nat Med* **10:** 871–5.
8. Tsunetsugu-Yokota Y., Ohnishi K., Takemori T. (2006) Severe acute respiratory syndrome (SARS) coronavirus: application of monoclonal antibodies and development of an effective vaccine. *Rev Med Virol* **16:** 117–31.
9. Sui J., Li W., Roberts A., Matthews L.J., Murakami A., Vogel L. *et al.* (2005) Evaluation of human monoclonal antibody 80R for

immunoprophylaxis of severe acute respiratory syndrome by an animal study, epitope mapping, and analysis of spike variants. *J Virol* **79:** 5900–6.
10. Matsuyama S., Ujike M., Morikawa S., Tashiro M., Taguchi F. (2005) Protease-mediated enhancement of severe acute respiratory syndrome coronavirus infection. *Proc Natl Acad Sci USA* **102:** 12543–7.
11. Ami Y., Nagata N., Shirato K., Watanabe R., Iwata N., Nakagaki K. *et al.* (2008) Co-infection of respiratory bacterium with severe acute respiratory syndrome coronavirus induces an exacerbated pneumonia in mice. *Microbiol Immunol* **52:** 118–27.
12. Tsunetsugu-Yokota Y., Ato M., Takahashi Y., Hashimoto S., Kaji T., Kuraoka M. *et al.* (2007) Formalin-treated UV-inactivated SARS coronavirus vaccine retains its immunogenicity and promotes Th2-type immune responses. *Jpn J Infect Dis* **60:** 106–12.
13. Ishii K., Hasegawa H., Nagata N., Mizutani T., Morikawa S., Suzuki T. *et al.* (2006) Induction of protective immunity against severe acute respiratory syndrome coronavirus (SARS-CoV) infection using highly attenuated recombinant vaccinia virus DIs. *Virology* **351:** 368–80.
14. Takasuka N., Fujii H., Takahashi Y., Kasai M., Morikawa S., Itamura S. *et al.* (2004) A subcutaneously injected UV-inactivated SARS coronavirus vaccine elicits systemic humoral immunity in mice. *Int Immunol* **16:** 1423–30.
15. Fukushi S., Mizutani T., Saijo M., Kurane I., Taguchi F., Tashiro M. *et al.* (2006) Evaluation of a novel vesicular stomatitis virus pseudotype-based assay for detection of neutralizing antibody responses to SARS-CoV. *J Med Virol* **78:** 1509–12.
16. Nagata N., Iwata N., Hasegawa H., Fukushi S., Yokoyama M., Harashima A. *et al.* (2007) Participation of both host and virus factors in induction of severe acute respiratory syndrome (SARS) in F344 rats infected with SARS coronavirus. *J Virol* **81:** 1848–57.
17. Ohnishi K., Sakaguchi M., Kaji T., Akagawa K., Taniyama T., Kasai M. *et al.* (2005) Immunological detection of severe acute respiratory syndrome coronavirus by monoclonal antibodies. *Jpn J Infect Dis* **58:** 88–94.
18. Mitsuki Y.Y., Ohnishi K., Takagi H., Oshima M., Yamamoto T., Mizukoshi F. *et al.* (2008) A single amino acid substitution in the S1 and S2 Spike protein domains determines the neutralization escape phenotype of SARS-CoV. *Microbes Infect.*
19. Wong V.W., Dai D., Wu A.K., Sung J.J. (2003) Treatment of severe acute respiratory syndrome with convalescent plasma. *Hong Kong Med J* **9:** 199–201.
20. Subbarao K., McAuliffe J., Vogel L., Fahle G., Fischer S., Tatti K. *et al.* (2004) Prior infection and passive transfer of neutralizing antibody prevent replication of severe acute respiratory syndrome coronavirus in the respiratory tract of mice. *J Virol* **78:** 3572–7.
21. Sui J., Li W., Murakami A., Tamin A., Matthews L.J., Wong S.K. *et al.* (2004) Potent neutralization of severe acute respiratory syndrome (SARS) coronavirus by a human mAb to S1 protein that blocks receptor association. *Proc Natl Acad Sci USA* **101:** 2536–41.
22. Rockx B., Corti D., Donaldson E., Sheahan T., Stadler K., Lanzavecchia A. *et al.* (2008) Structural basis for potent cross-neutralizing human monoclonal antibody protection against lethal human and zoonotic severe acute respiratory syndrome coronavirus challenge. *J Virol* **82:** 3220–35.
23. Zhu Z., Chakraborti S., He Y., Roberts A., Sheahan T., Xiao X. *et al.* (2007) Potent cross-reactive neutralization of SARS coronavirus isolates by human monoclonal antibodies. *Proc Natl Acad Sci USA* **104:** 12 123–8.
24. McCray P.B., Jr., Pewe L., Wohlford-Lenane C., Hickey M., Manzel L., Shi L. *et al.* (2007) Lethal infection of K18-hACE2 mice infected with severe acute respiratory syndrome coronavirus. *J Virol* **81:** 813–21.
25. Roberts A., Deming D., Paddock C.D., Cheng A., Yount B., Vogel L. *et al.* (2007) A mouse-adapted SARS-coronavirus causes disease and mortality in BALB/c mice. *PLoS Pathog* **3:** e5.
26. Tseng C.T., Huang C., Newman P., Wang N., Narayanan K., Watts D.M. *et al.* (2007) Severe acute respiratory syndrome coronavirus infection of mice transgenic for the human Angiotensin-converting enzyme 2 virus receptor. *J Virol* **81:** 1162–73.

JOURNAL OF VIROLOGY, Mar. 2009, p. 2389–2392 Vol. 83, No. 5
0022-538X/09/$08.00+0 doi:10.1128/JVI.01690-08

Proteasomal Turnover of Hepatitis C Virus Core Protein Is Regulated by Two Distinct Mechanisms: a Ubiquitin-Dependent Mechanism and a Ubiquitin-Independent but PA28γ-Dependent Mechanism▽

Ryosuke Suzuki,[1] Kohji Moriishi,[2] Kouichirou Fukuda,[1] Masayuki Shirakura,[1] Koji Ishii,[1] Ikuo Shoji,[3] Takaji Wakita,[1] Tatsuo Miyamura,[1] Yoshiharu Matsuura,[2] and Tetsuro Suzuki[1]*

Department of Virology II, National Institute of Infectious Diseases, Tokyo 162-8640,[1] Department of Molecular Virology, Research Institute for Microbial Diseases, Osaka University, Osaka 565-0871,[2] and Division of Microbiology, Kobe University Graduate School of Medicine, Hyogo 650-0017,[3] Japan

Received 8 August 2008/Accepted 5 December 2008

We have previously reported on the ubiquitylation and degradation of hepatitis C virus core protein. Here we demonstrate that proteasomal degradation of the core protein is mediated by two distinct mechanisms. One leads to polyubiquitylation, in which lysine residues in the N-terminal region are preferential ubiquitylation sites. The other is independent of the presence of ubiquitin. Gain- and loss-of-function analyses using lysineless mutants substantiate the hypothesis that the proteasome activator PA28γ, a binding partner of the core, is involved in the ubiquitin-independent degradation of the core protein. Our results suggest that turnover of this multifunctional viral protein can be tightly controlled via dual ubiquitin-dependent and -independent proteasomal pathways.

Hepatitis C virus (HCV) core protein, whose amino acid sequence is highly conserved among different HCV strains, not only is involved in the formation of the HCV virion but also has a number of regulatory functions, including modulation of signaling pathways, cellular and viral gene expression, cell transformation, apoptosis, and lipid metabolism (reviewed in references 9 and 15). We have previously reported that the E6AP E3 ubiquitin (Ub) ligase binds to the core protein and plays an important role in polyubiquitylation and proteasomal degradation of the core protein (22). Another study from our group identified the proteasome activator PA28γ/REG-γ as an HCV core-binding partner, demonstrating degradation of the core protein via a PA28γ-dependent pathway (16, 17). In this work, we further investigated the molecular mechanisms underlying proteasomal degradation of the core protein and found that in addition to regulation by the Ub-mediated pathway, the turnover of the core protein is also regulated by PA28γ in a Ub-independent manner.

Although ubiquitylation of substrates generally requires at least one Lys residue to serve as a Ub acceptor site (5), there is no consensus as to the specificity of the Lys targeted by Ub (4, 8). To determine the sites of Ub conjugation in the core protein, we used site-directed mutagenesis to replace individual Lys residues or clusters of Lys residues with Arg residues in the N-terminal 152 amino acids (aa) of the core (C152), within which is contained all seven Lys residues (Fig. 1A). Plasmids expressing a variety of mutated core proteins were generated by PCR and inserted into the pCAGGS (18). Each core-expressing construct was transfected into human embryonic kidney 293T cells along with the pMT107 (25) encoding a Ub moiety tagged with six His residues (His_6). Transfected cells were treated with the proteasome inhibitor MG132 for 14 h to maximize the level of Ub-conjugated core intermediates by blocking the proteasome pathway and were harvested 48 h posttransfection. His_6-tagged proteins were purified from the extracts by Ni^{2+}-chelation chromatography. Eluted protein and whole lysates of transfected cells before purification were analyzed by Western blotting using anticore antibodies (Fig. 1B). Mutations replacing one or two Lys residues with Arg in the core protein did not affect the efficiency of ubiquitylation: detection of multiple Ub-conjugated core intermediates was observed in the mutant core proteins comparable to the results seen with the wild-type core protein as previously reported (23). In contrast, a substitution of four N-terminal Lys residues (C152K6-23R) caused a significant reduction in ubiquitylation (Fig. 1B, lane 9). Multiple Ub-conjugated core intermediates were not detected in the Lys-less mutant (C152KR), in which all seven Lys residues were replaced with Arg (Fig. 1B, lane 11). These results suggest that there is not a particular Lys residue in the core protein to act as the Ub acceptor but that more than one Lys located in its N-terminal region can serve as the preferential ubiquitylation site. In rare cases, Ub is known to be conjugated to the N terminus of proteins; however, these results indicate that this does not occur within the core protein.

To investigate how polyubiquitylation correlates with proteasome degradation of the core protein, we performed kinetic analysis of the wild-type and mutated core proteins by use of the Ub protein reference (UPR) technique, which can compensate for data scatter of sample-to-sample variations such as levels of expression (10, 24). Fusion proteins expressed from UPR-based constructs (Fig. 2A) were cotranslationally cleaved by deubiquitylating enzymes, thereby generating equimolar quantities of the core proteins and the reference protein, dihydrofolate reductase-hemagglutinin (DHFR-HA) tag-modified Ub, in which the Lys at aa 48 was replaced by Arg to prevent its polyubiquitylation (Ub^{R48}). After 24 h of transfec-

* Corresponding author. Mailing address: Department of Virology II, National Institute of Infectious Diseases, 1-23-1 Toyama, Shinjuku-ku, Tokyo 162-8640, Japan. Phone: 81-3-5285-1111. Fax: 81-3-5285-1161. E-mail: tesuzuki@nih.go.jp.

▽ Published ahead of print on 17 December 2008.

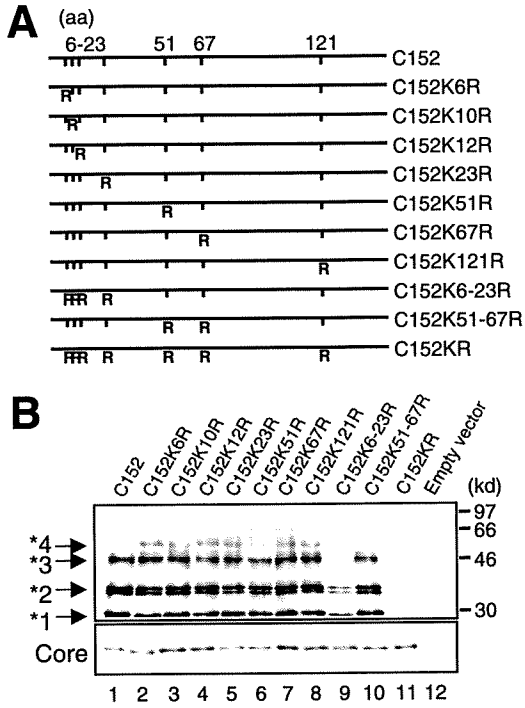

FIG. 1. In vivo ubiquitylation of HCV core protein. (A) The HCV core protein (N-terminal 152 aa) is represented on the top. The positions of the amino acid residues of the core protein are indicated above the bold lines. The positions of the seven Lys residues in the core are marked by vertical ticks. Substitution of Lys with Arg (R) is schematically depicted. (B) Detection of ubiquitylated forms of the core proteins. The transfected cells with core expression plasmids and pMT107 were treated with the proteasome inhibitor MG132 and harvested 48 h after transfection. His_6-tagged proteins were purified and subsequently analyzed by Western blot analysis using anticore antibody (upper panel). Core proteins conjugated to a number of His_6-Ub are denoted with asterisks. Whole lysates of transfected cells before purification were also analyzed (lower panel). Lanes 1 to 11, C152 to C152KR, as indicated for panel A. Lane 12; empty vector.

tion with UPR constructs, cells were treated with cycloheximide and the amounts of core proteins and DHFR-HA-Ub^{R48} at the indicated time points were determined by Western blot analysis using anticore and anti-HA antibodies. The mature form of the core protein, aa 1 to 173 (C173) (13, 20), and C152 were degraded with first-order kinetics (Fig. 2B and D). MG132 completely blocked the degradation of C173 and C152 (Fig. 2B), and C152K6-23R and C152KR were markedly stabilized (Fig. 2C). The half-lives of C173 and C152 were calculated to be 5 to 6 h, whereas those of C152K6-23R and C152KR were calculated to be 22 to 24 h (Fig. 2D), confirming that the Ub plays an important role in regulating degradation of the core protein. Nevertheless, these results also suggest possible involvement of the Ub-independent pathway in the turnover of the core protein, as C152KR is more destabilized than the reference protein (Fig. 2C and 2D).

We have shown that PA28γ specifically binds to the core protein and is involved in its degradation (16, 17). Recent studies demonstrated that PA28γ is responsible for Ub-independent degradation of the steroid receptor coactivator SRC-3 and cell cycle inhibitors such as p21 (3, 11, 12). Thus, we next investigated the possibility of PA28γ involvement in the deg-

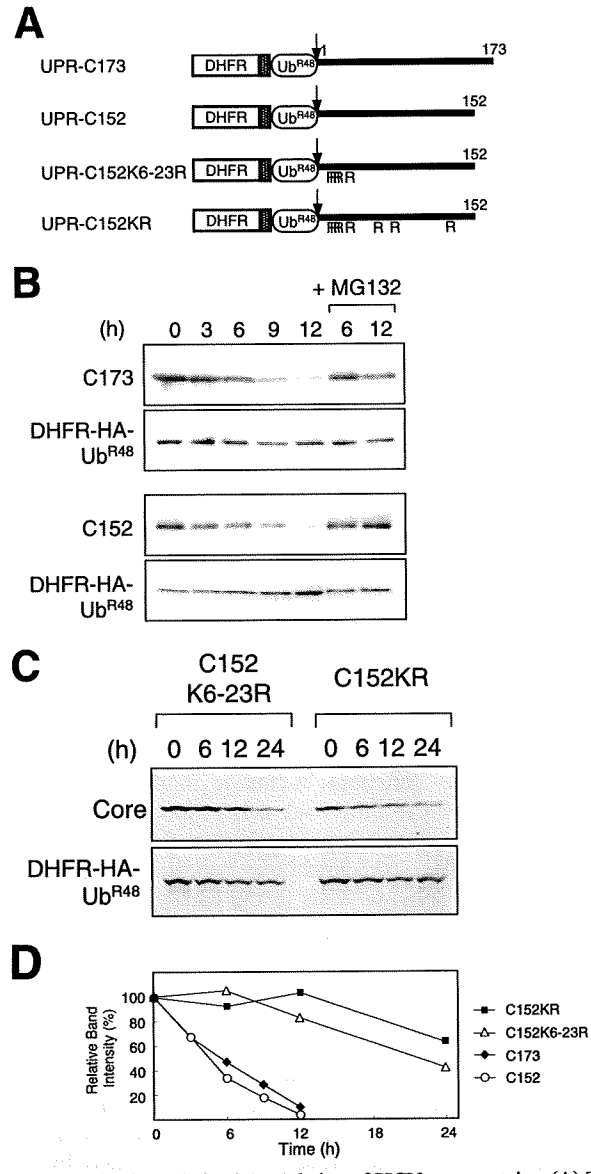

FIG. 2. Kinetic analysis of degradation of HCV core proteins. (A) The fusion constructs used in the UPR technique. Open boxes indicate the DHFR sequence, which is extended at the C terminus by a sequence containing the HA epitope (hatched boxes). Ub^{R48} moieties bearing the Lys-Arg substitution at aa 48 are represented by open ellipses. Bold lines indicate the regions of the core protein. The amino acid positions of the core protein are indicated above the bold lines. The arrows indicate the sites of in vivo cleavage by deubiquitylating enzymes. (B and C) Turnover of the core proteins. After a 24-h transfection with each UPR construct, cells were treated with 50 μg of cycloheximide/ml in the presence or absence of 10 μM MG132 for the different time periods indicated. Cells were lysed at the different time points indicated, followed by evaluation via sodium dodecyl sulfate-polyacrylamide gel electrophoresis and Western blot analysis using antibodies against the core protein and HA. (D) Quantitation of the data shown in panels B and C. At each time point, the ratio of band intensity of the core protein relative to the reference DHFR-HA-Ub^{R48} was determined by densitometry and is plotted as a percentage of the ratio at time zero.

radation of either C152KR or C152. Since C152KR carries two amino acid substitutions in the PA28γ-binding region (aa 44 to 71) (17), we tested the influence of the mutations of C152KR on the interaction with PA28γ by use of a coimmunoprecipi-

tation assay. When Flag-tagged PA28γ (F-PA28γ) was expressed in cells along with C152 or C152KR, F-PA28γ precipitated along with both C152 and C152KR, indicating that PA28γ interacts with both core proteins (Fig. 3A). Figure 3B reveals the effect of exogenous expression of F-PA28γ on the steady-state levels of C152 and C152KR. Consistent with previous data (17), the expression level of C152 was decreased to a nearly undetectable level in the presence of PA28γ (Fig. 3B, lanes 1 and 3). Interestingly, exogenous expression of PA28γ led to a marked reduction in the amount of C152KR expressed (Fig. 3B, lanes 5 and 7). Treatment with MG132 increased the steady-state level of the C152KR in the presence of F-PA28γ as well as the level of C152 (Fig. 3B, lanes 4 and 8).

We further investigated whether PA28γ affects the turnover of Lys-less core protein through time course experiments. C152KR was rapidly destabilized and almost completely degraded in a 3-h chase experiment using cells overexpressing F-PA28γ (Fig. 3C, left panels). A similar result was obtained using an analogous Lys-less mutant of the full-length core protein C191KR (Fig. 3C, right panels), thus demonstrating that the Lys-less core protein undergoes proteasomal degradation in a PA28γ-dependent manner. These results suggest that PA28γ may play a role in accelerating the turnover of the HCV core protein that is independent of ubiquitylation.

Finally, we examined gain- and loss-of-function of PA28γ with respect to degradation of full-length wild-type (C191) and mutated (C191KR) core proteins in human hepatoma Huh-7 cells. As expected, exogenous expression of PA28γ or E6AP caused a decrease in the C191 steady-state levels (Fig. 4A). In contrast, the C191KR level was decreased with expression of PA28γ but not of E6AP. We further used RNA interference to inhibit expression of PA28γ or E6AP. An increase in the abundance of C191KR was observed with PA28γ small interfering RNA (siRNA) but not with E6AP siRNA (Fig. 4B). An increase in the C191 level caused by the activity of siRNA against PA28γ or E6AP was confirmed as well.

Taking these results together, we conclude that turnover of the core protein is regulated by both Ub-dependent and Ub-independent pathways and that PA28γ is possibly involved in Ub-independent proteasomal degradation of the core protein. PA28 is known to specifically bind and activate the 20S proteasome (19). Thus, PA28γ may function by facilitating the delivery of the core protein to the proteasome in a Ub-independent manner.

Accumulating evidence suggests the existence of proteasome-dependent but Ub-independent pathways for protein degradation, and several important molecules, such as p53, p73, Rb, SRC-3, and the hepatitis B virus X protein, have two distinct degradation pathways that function in a Ub-dependent and Ub-independent manner (1, 2, 6, 7, 14, 21, 27). Recently, critical roles for PA28γ in the Ub-independent pathway have been demonstrated; SRC-3 and p21 can be recognized by the 20S proteasome independently of ubiquitylation through their interaction with PA28γ (3, 11, 12). It has also been reported that phosphorylation-dependent ubiquitylation mediated by GSK3 and SCF is important for SRC-3 turnover (26). Nevertheless, the precise mechanisms underlying turnover of most of the proteasome substrates that are regulated in both Ub-dependent and Ub-independent manners are not well understood. To our knowledge, the HCV core protein is the first

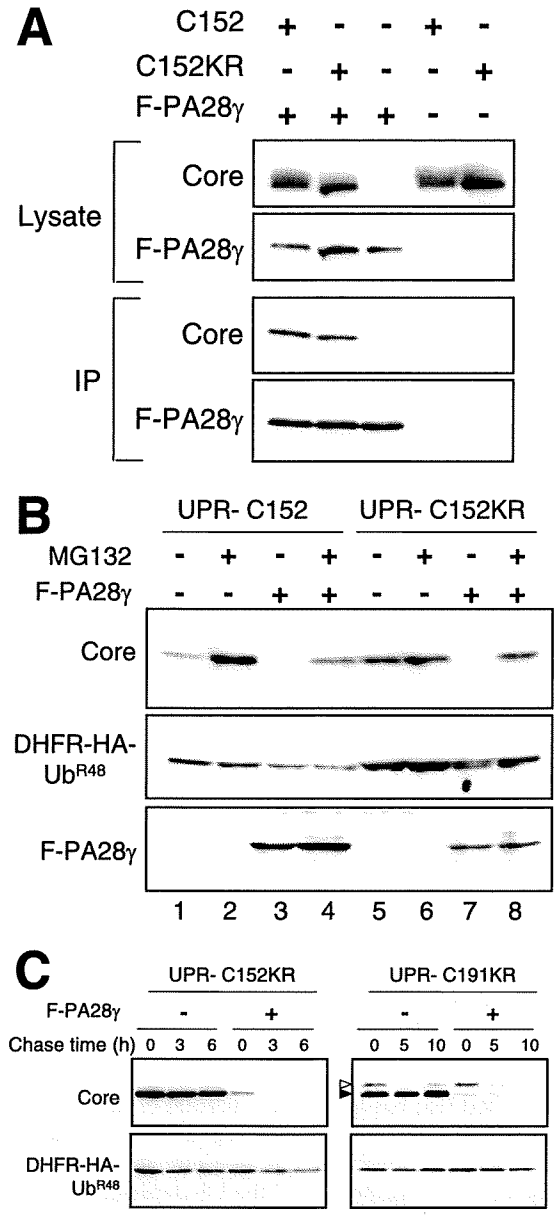

FIG. 3. PA28γ-dependent degradation of the core protein. (A) Interaction of the core protein with PA28γ. Cells were cotransfected with the wild-type (C152) or Lys-less (C152KR) core expression plasmid in the presence of a Flag-PA28γ (F-PA28γ) expression plasmid or an empty vector. The transfected cells were treated with MG132. After 48 h, the cell lysates were immunoprecipitated with anti-Flag antibody and visualized by Western blotting with anticore antibodies. Western blot analysis of whole cell lysates was also performed. (B) Degradation of the wild-type and Lys-less core proteins via the PA28γ-dependent pathway. Cells were transfected with the UPR construct with or without F-PA28γ. In some cases, cells were treated with 10 μM MG132 for 14 h before harvesting. Western blot analysis was performed using anticore, anti-HA, and anti-Flag antibodies. (C) After 24 h of transfection with UPR-C152KR and UPR-C191KR with or without F-PA28γ (an empty vector), cells were treated with 50 μg of cycloheximide/ml for different time periods as indicated (chase time). Western blot analysis was performed using anticore and anti-HA antibodies. The precursor core protein and the core that was processed, presumably by signal peptide peptidase, are denoted by open and closed triangles, respectively.

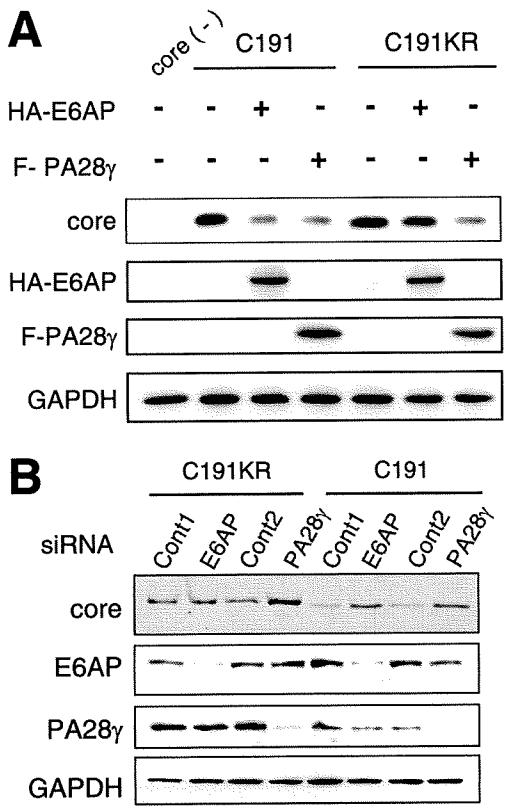

FIG. 4. Ub-dependent and Ub-independent degradation of the full-length core protein in hepatic cells. (A) Huh-7 cells were cotransfected with plasmids for the full-length core protein (C191) or its Lys-less mutant (C191KR) in the presence of F-PA28γ or HA-tagged-E6AP expression plasmid (HA-E6AP). After 48 h, cells were lysed and Western blot analysis was performed using anticore, anti-HA, anti-Flag, or anti-GAPDH. (B) Huh-7 cells were cotransfected with core expression plasmids along with siRNA against PA28γ or E6AP or with negative control siRNA. Cells were harvested 72 h after transfection and subjected to Western blot analysis.

viral protein studied that has led to identification of key cellular factors responsible for proteasomal degradation via dual distinct mechanisms. Although the question remains whether there is a physiological significance of the Ub-dependent and Ub-independent degradation of the core protein, it is reasonable to consider that tight control over cellular levels of the core protein, which is multifunctional and essential for viral replication, maturation, and pathogenesis, may play an important role in representing the potential for its functional activity.

This work was supported by a grant-in-aid for Scientific Research from the Japan Society for the Promotion of Science, from the Ministry of Health, Labor and Welfare of Japan, and from the Ministry of Education, Culture, Sports, Science and Technology, by Research on Health Sciences focusing on Drug Innovation from the Japan Health Sciences Foundation, Japan, and by the Program for Promotion of Fundamental Studies in Health Sciences of the National Institute of Biomedical Innovation of Japan.

REFERENCES

1. **Asher, G., J. Lotem, L. Sachs, C. Kahana, and Y. Shaul.** 2002. Mdm-2 and ubiquitin-independent p53 proteasomal degradation regulated by NQO1. Proc. Natl. Acad. Sci. USA **99:**13125–13130.
2. **Asher, G., P. Tsvetkov, C. Kahana, and Y. Shaul.** 2005. A mechanism of ubiquitin-independent proteasomal degradation of the tumor suppressors p53 and p73. Genes Dev. **19:**316–321.
3. **Chen, X., L. F. Barton, Y. Chi, B. E. Clurman, and J. M. Roberts.** 2007. Ubiquitin-independent degradation of cell-cycle inhibitors by the REGγ proteasome. Mol. Cell **26:**843–852.
4. **Ciechanover, A.** 1998. The ubiquitin-proteasome pathway: on protein death and cell life. EMBO J. **17:**7151–7160.
5. **Hershko, A., A. Ciechanover, and A. Varshavsky.** 2000. The ubiquitin system. Nat. Med. **6:**1073–1081.
6. **Jariel-Encontre, I., M. Pariat, F. Martin, S. Carillo, C. Salvat, and M. Piechaczyk.** 1995. Ubiquitinylation is not an absolute requirement for degradation of c-Jun protein by the 26 S proteasome. J. Biol. Chem. **270:**11623–11627.
7. **Jin, Y., H. Lee, S. X. Zeng, M. S. Dai, and H. Lu.** 2003. MDM2 promotes p21waf1/cip1 proteasomal turnover independently of ubiquitylation. EMBO J. **22:**6365–6377.
8. **Ju, D., and Y. Xie.** 2006. Identification of the preferential ubiquitination site and ubiquitin-dependent degradation signal of Rpn4. J. Biol. Chem. **281:**10657–10662.
9. **Lai, M. M. C., and C. F. Ware.** 1999. Hepatitis C virus core protein: possible roles in viral pathogenesis. Springer, Berlin, Germany.
10. **Lévy, F., N. Johnsson, T. Rumenapf, and A. Varshavsky.** 1996. Using ubiquitin to follow the metabolic fate of a protein. Proc. Natl. Acad. Sci. USA **93:**4907–4912.
11. **Li, X., L. Amazit, W. Long, D. M. Lonard, J. J. Monaco, and B. W. O'Malley.** 2007. Ubiquitin- and ATP-independent proteolytic turnover of p21 by the REGγ-proteasome pathway. Mol. Cell **26:**831–842.
12. **Li, X., D. M. Lonard, S. Y. Jung, A. Malovannaya, Q. Feng, J. Qin, S. Y. Tsai, M. J. Tsai, and B. W. O'Malley.** 2006. The SRC-3/AIB1 coactivator is degraded in a ubiquitin- and ATP-independent manner by the REGγ proteasome. Cell **124:**381–392.
13. **Liu, Q., C. Tackney, R. A. Bhat, A. M. Prince, and P. Zhang.** 1997. Regulated processing of hepatitis C virus core protein is linked to subcellular localization. J. Virol. **71:**657–662.
14. **Lonard, D. M., Z. Nawaz, C. L. Smith, and B. W. O'Malley.** 2000. The 26S proteasome is required for estrogen receptor-α and coactivator turnover and for efficient estrogen receptor-α transactivation. Mol. Cell **5:**939–948.
15. **Moradpour, D., F. Penin, and C. M. Rice.** 2007. Replication of hepatitis C virus. Nat. Rev. Microbiol. **5:**453–463.
16. **Moriishi, K., R. Mochizuki, K. Moriya, H. Miyamoto, Y. Mori, T. Abe, S. Murata, K. Tanaka, T. Miyamura, T. Suzuki, K. Koike, and Y. Matsuura.** 2007. Critical role of PA28γ in hepatitis C virus-associated steatogenesis and hepatocarcinogenesis. Proc. Natl. Acad. Sci. USA **104:**1661–1666.
17. **Moriishi, K., T. Okabayashi, K. Nakai, K. Moriya, K. Koike, S. Murata, T. Chiba, K. Tanaka, R. Suzuki, T. Suzuki, T. Miyamura, and Y. Matsuura.** 2003. Proteasome activator PA28γ-dependent nuclear retention and degradation of hepatitis C virus core protein. J. Virol. **77:**10237–10249.
18. **Niwa, H., K. Yamamura, and J. Miyazaki.** 1991. Efficient selection for high-expression transfectants with a novel eukaryotic vector. Gene **108:**193–199.
19. **Realini, C., C. C. Jensen, Z. Zhang, S. C. Johnston, J. R. Knowlton, C. P. Hill, and M. Rechsteiner.** 1997. Characterization of recombinant REGα, REGβ, and REGγ proteasome activators. J. Biol. Chem. **272:**25483–25492.
20. **Santolini, E., G. Migliaccio, and N. La Monica.** 1994. Biosynthesis and biochemical properties of the hepatitis C virus core protein. J. Virol. **68:**3631–3641.
21. **Sheaff, R. J., J. D. Singer, J. Swanger, M. Smitherman, J. M. Roberts, and B. E. Clurman.** 2000. Proteasomal turnover of p21Cip1 does not require p21Cip1 ubiquitination. Mol. Cell **5:**403–410.
22. **Shirakura, M., K. Murakami, T. Ichimura, R. Suzuki, T. Shimoji, K. Fukuda, K. Abe, S. Sato, M. Fukasawa, Y. Yamakawa, M. Nishijima, K. Moriishi, Y. Matsuura, T. Wakita, T. Suzuki, P. M. Howley, T. Miyamura, and I. Shoji.** 2007. E6AP ubiquitin ligase mediates ubiquitylation and degradation of hepatitis C virus core protein. J. Virol. **81:**1174–1185.
23. **Suzuki, R., K. Tamura, J. Li, K. Ishii, Y. Matsuura, T. Miyamura, and T. Suzuki.** 2001. Ubiquitin-mediated degradation of hepatitis C virus core protein is regulated by processing at its carboxyl terminus. Virology **280:**301–309.
24. **Suzuki, T., and A. Varshavsky.** 1999. Degradation signals in the lysine-asparagine sequence space. EMBO J. **18:**6017–6026.
25. **Treier, M., L. M. Staszewski, and D. Bohmann.** 1994. Ubiquitin-dependent c-Jun degradation in vivo is mediated by the δ domain. Cell **78:**787–798.
26. **Wu, R. C., Q. Feng, D. M. Lonard, and B. W. O'Malley.** 2007. SRC-3 coactivator functional lifetime is regulated by a phospho-dependent ubiquitin time clock. Cell **129:**1125–1140.
27. **Zhang, Z., and R. Zhang.** 2008. Proteasome activator PA28γ regulates p53 by enhancing its MDM2-mediated degradation. EMBO J. **27:**852–864.

Gene 432 (2009) 60–66

Contents lists available at ScienceDirect

Gene

journal homepage: www.elsevier.com/locate/gene

Molecular cloning and characterization of the common marmoset huntingtin gene

Hirohiko Hohjoh [a,*], Hirofumi Akari [b], Yuko Fujiwara [a,c], Yoshiko Tamura [a], Hirohisa Hirai [d], Keiji Wada [c]

[a] Department of Molecular Genetics, National Institute of Neuroscience, NCNP, 4-1-1 Ogawahigashi, Kodaira, Tokyo 187-8502, Japan
[b] Laboratory of Disease Control, Tsukuba Primate Research Center, National Institute of Biomedical Innovation, Tsukuba, Ibaraki, Japan
[c] Department of Degenerative Neurological Diseases, National Institute of Neuroscience, NCNP, Kodaira, Tokyo, Japan
[d] Primate Research Institute, Kyoto University, Inuyama, Aichi, Japan

ARTICLE INFO

Article history:
Received 24 July 2008
Received in revised form 4 November 2008
Accepted 5 November 2008
Available online 24 November 2008

Received by M. Di Giulio

Keywords:
Common marmoset
Huntingtin
Gene silencing
Immortalized cell line

ABSTRACT

We report here for the first time the isolation and identification of the common marmoset (*Callithrix jacchus*) *huntingtin* (*Htt*) gene, whose ortholog in humans is known to be related to Huntington's disease (HD). A 9396 nucleotide complementary DNA (cDNA) carrying the putative full-length open reading frame of the marmoset *Htt* gene was identified, and highly conserved nucleotide and amino acid sequences among primates were observed. Based on this data and using tools evaluated for the detection of the marmoset *Htt* gene, we have demonstrated gene silencing against the expression of endogenous *Htt* gene in immortalized common marmoset mononuclear cells by means of RNA interference (RNAi). Taken together, the data presented here may assist us in realizing a non-human primate HD model with the common marmoset.

1. Introduction

Huntington's disease (HD) is an autosomal dominant neurodegenerative disease characterized by progressive and selective neural cell death associated with choreic movement and dementia (Walker, 2007). The responsible gene for HD, the huntingtin (Htt) gene, has been identified on chromosome 4q16.3 (Gusella et al., 1983; Gilliam et al., 1987), and an aberrant length of a CAG triplet repeat in exon 1, followed by expanded tracts of polyglutamine in the Htt polypeptide, is greatly involved in the onset of HD (Huntington's-Disease, 1993). Although the molecular mechanisms of either normal or aberrant Htt protein are still poorly understood, HD model animals (Mangiarini et al., 1996; Kazemi-Esfarjani and Benzer, 2000; von Horsten et al., 2003) and cells (Lunkes and Mandel, 1998) for understanding the pathogenesis of HD and developing therapies have been established by means of genetic engineering based on the genetic information of *Htt*. The use of an animal model that is closely related to humans may be particularly promising.

The common marmoset (*Callithrix jacchus*) is classified into the Callitrichidae family of Platyrrini (New World monkeys) and has been used as a non-human primate experimental animal in various research fields including gene therapy, autoimmune disease, organ transplantation, and pharmacology (Kendall et al., 1998; Doods et al., 2000; Deisboeck et al., 2003; t'Hart et al., 2003). Accordingly, it is worth promoting studies with the common marmoset aimed at overcoming neurodegenerative diseases such as HD, as the animal's close relationship to humans makes it well suited to this kind of study. Indeed, a recent study has generated a non-human primate HD model with the rhesus monkey (*Macaca mulatta*) (Palfi et al., 2007; Yang et al., 2008).

In this report, we describe for the first time the isolation and characterization of a cDNA encoding the putative full-length open reading frame of the common marmoset *Htt* gene, and present experimental data based on the isolated cDNA. The data presented here may provide us with useful information for establishing non-human primate HD models with the common marmoset.

2. Materials and methods

2.1. Preparation of total RNA

Common marmoset total RNA was isolated from the brain tissue of a stillborn marmoset fetus and immortalized monocytes (described below) using Trizol (Invitrogen). The experiments with the common marmoset complied with protocols approved by the ethical committee for primate research of the National Center of Neurology and Psychiatry and adhered to the legal requirements of Japan.

Abbreviations: HD, Huntington's disease; Htt, huntingtn; RNAi, RNA interference; cDNA, complementary DNA; PBMC, peripheral blood mononuclear cell; RT, reverse transcription; PCR, polymerase chain reaction; ORF, open reading frame; APP, amyloid precursor protein; GAPDH, glyceraldehyde-3-phosphate dehydrogenase; GFP, green fluorescence protein; CMV, Cytomegalovirus.

* Corresponding author.
E-mail address: hohjohh@ncnp.go.jp (H. Hohjoh).

0378-1119/$ – see front matter © 2008 Elsevier B.V. All rights reserved.
doi:10.1016/j.gene.2008.11.012

2.2. Established common marmoset cell lines

Adult common marmosets being reared at the Primate Research Institute of Kyoto University or Tsukuba Primate Research Center were anesthetized by ketamine, which was approved by the Animal Welfare and Animal Care Committees of both institutes, and peripheral blood was collected. From the collected blood samples, peripheral blood mononuclear cells (PBMCs) were purified and immortalized by infection of a 488-77 strain of *Herpesvirus saimiri* (kindly provided by Dr. R. C. Desrosiers) as previously described (Akari et al., 1996). The established marmoset cell lines, designated HSCj-110, HSCj-009, and HSCj-002, were phenotypically activated CD3+T lymphocytic cells and grown in RPMI-1640 medium (Sigma) supplemented with 10% FCS, 50 mM 2-mercaptoethanol, and antibiotics.

2.3. Reverse transcription – (real time) polymerase chain reaction [RT-(real time) PCR]

The common marmoset total RNAs were subjected to complementary DNA (cDNA) synthesis using oligo(dT) primers and a Superscript III reverse transcriptase (Invitrogen), according to the manufacturer's instructions, and polymerase chain reaction (PCR) using the cDNAs as templates was carried out by means of the ABI GeneAmp PCR system 9700 (Applied Biosystems). In the case of real time PCR, the cDNAs were examined by the AB 7300 Real Time PCR System (Applied Biosystems) with a TaqMan Universal PCR Master Mix together with Assays-on-Demand Gene Expression products (Applied Biosystems) or a SYBR Green PCR Master Mix together with Perfect Real Time Primers (Takara Bio) or designed PCR primers, according to the manufacturers' instructions. Synthesized oligonucleotide primers and purchased primer and probe were as follows:

Synthesized oligonucleotide primers:

HD1-F: 5′-TATAGAATTCGGGAGACCGCCATGGCGAC-3′
HD1-ORF-R: 5′-TCAAGCGGCCGCTCAGCAGGTGGTGACCTTG-3′
HD1-1900R2: 5′-TAAAGGATCCCCGTCTAACACAATTTCAG-3′
cjHtt(1139)-F: 5′-TTATAGCTGGAGGCGGTTCC-3′
cjHtt(1254)-R: 5′-GACGTCCGACCTCGATTCAG-3′

Purchased primer and probe:

Assays-on-Demand Gene Expression product for the human *Htt* gene (Assay ID: Hs00169273_m1) (Applied Biosystems).

Perfect Real Time Primers for the human *GAPDH* gene (Primer-Set ID: HA067812) (Takara Bio).

2.4. Cloning and sequence analysis of the full-length ORF of the marmoset Htt gene

Complementary DNA derived from the common marmoset total RNA was subjected to PCR amplification using *TaKaRa LA Taq* polymerase (TAKARA BIO) with the HD1-F and HD1-ORF-R primers under the following thermal cycling conditions: heat denaturation at 94 °C for 1 min, 30 cycles of amplification including denaturation at 94 °C for 20 s and extension at 68 °C for 12 min, and a final extension at 72 °C for 10 min. The PCR product was examined by agarose gel electrophoresis followed by ethidium bromide staining, and an approximately 9.4 kb PCR band (Fig. 1) was purified from the gels using a TOPO XL gel purification kit (Invitrogen). The resultant PCR product was inserted into the pCR-XL-TOPO plasmid with a TOPO XL PCR cloning kit (Invitrogen) and then sequence determination of the insert was carried out. To clarify uncertain nucleotide sequences, additional RT-PCR targeting of uncertain regions followed by sequence determination was performed and the precise nucleotide sequence was confirmed. The determined nucleotide sequence encoding a putative full-length ORF of the common marmoset *Htt* gene has been registered in the GenBank database: accession number, AB443866.

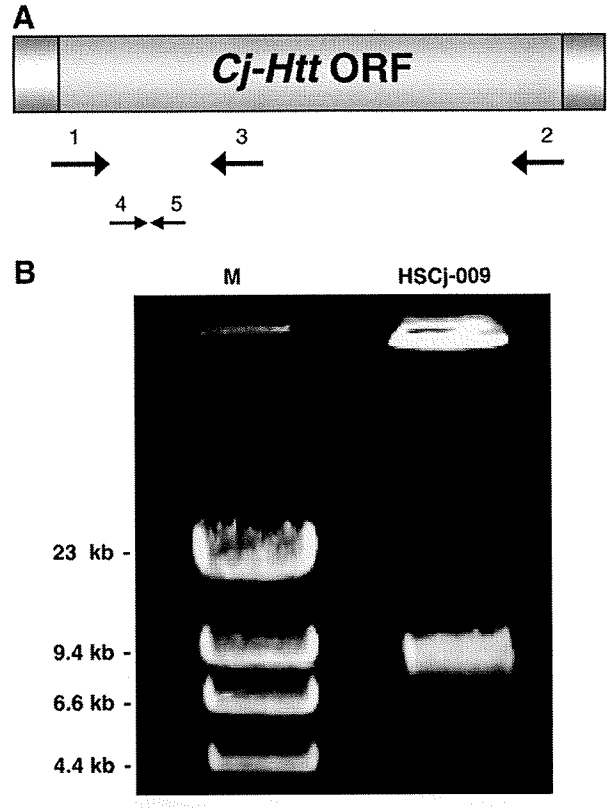

Fig. 1. RT-PCR amplification. (A) Schematic drawing of putative *Htt* cDNA. Open reading frame (ORF) is indicated by a yellow box. Arrows indicate synthesized PCR primers, which are designed in possibly conserved nucleotide sequences: 1, HD1-F; 2, HD1-ORF-R; 3, HD1-1900R2; 4, cjHtt(1139)-F; 5, cjHtt(1254)-R (detailed in Materials and methods). (B) RT-PCR. The first strand cDNA was synthesized by RT using RNA isolated from immortalized common marmoset mononuclear cells (HSCj-009) as a template and oligo(dT) as a primer. The following PCR was carried out using HD1-F and HD1-ORF-R primers. The resultant PCR products were analyzed by gel electrophoresis with 0.6 % agarose gel followed by ethidium bromide staining. Hind III-digested λDNA was used as a DNA size marker (M).

2.5. Western blotting

Equal amounts (~35 μg) of protein extracts from the common marmoset and mouse brain tissues and established PBMC lines (described above) were separated by SDS-PAGE with 5% polyacrylamide gels and electrophoretically blotted onto PVDF membranes (Millipore). Membranes were blocked for 1 h in blocking solution [5% non-fat milk in TBST buffer (25 mM Tris-HCl, pH 7.4, 150 mM NaCl and 0.1% Tween-20)] and incubated with 1/1000 dilution of mouse anti-huntingtin protein monoclonal antibodies [MAB2166 and MAB2170 (Chemicon); ab7666 (Abcam)] followed by washing in TBST buffer and further incubation with sheep anti-mouse Ig, HRP-linked whole Ab (GE Healthcare). Antigen-antibody complexes were visualized using ECL plus Western Blotting Detection Reagent (GE Healthcare). After detection of signals, the membranes were subjected to antibody removal in Re-Blot Plus strong antibody stripping solution (Chemicon) followed by washing in TBST buffer, and then incubated with 1/1000 dilution of mouse anti-APP [MAB348 (Chemicon)] monoclonal antibody. Subsequent processes were the same as described above.

2.6. Gene silencing of marmoset Htt by RNA interference

To monitor gene silencing against the common marmoset *Htt* gene, we constructed a reporter plasmid carrying the 5′-terminal region of the marmoset *Htt* linked with the *GFP* reporter gene: the PCR product obtained from RT-PCR with the HD1-F and HD1-1900R2 primers was

Table 1
Sequence homologies (%) among various species' *Htt* genes

Homo sapiens	*Callithrix jacchus*	*Canis lupus familiaris*	*Bos taurus*	*Sus scrofa*	*Mus musclus*	*Rattus norvegicus*
Homo sapiens	**95.1** **97.0**	87.0 92.0	84.0 89.5	84.1 88.6	86.1 91.2	85.8 91.2
Canis lupus familiaris		86.6 91.4	84.0 88.4	83.9 87.9	85.6 90.8	85.1 90.9
Callithrix jacchus			84.5 89.4	84.4 89.7	84.0 89.2	83.8 89.3
Bos taurus				86.8 89.3	81.2 87.1	81.3 87.4
Sus scrofa					80.9 86.9	80.8 87.2
Mus musclus						95.9 97.6
Rattus norvegicus						

Figures in upper and lower stands represent nucleotide and amino acid sequence homologies, respectively, between two species.

trimmed with EcoRI and BamHI, and inserted into the pd2EGFP-N1 plasmid (Clontech) treated with the same restriction enzymes. The resultant reporter (5′*Cj-Htt-GFP*) plasmid and synthetic siRNA duplex targeting the marmoset *Htt* (cjHtt-1 siRNA duplex) were cotransfected into mouse neuroblastoma Neuro2a cells by Lipofectamine 2000 transfection reagent (Invitrogen) as described previously (Sakai and Hohjoh, 2006). Two days after transfection, the cells were examined by a fluorescent microscope. When the endogenous marmoset *Htt* gene was inhibited by RNAi, the cjHtt-1 siRNA duplex (0.4 nmol/transfection) was introduced into HSCj-009 cells (1×10^6 cells/transfection) by means of a Nucleofector system (Amaxa Biosystems) according to the manufacturer's instructions. Two days after transfection, total RNA and cell lysate were prepared from the cells and examined by RT-real time PCR and Western blotting, respectively.

The nucleotide sequences of synthesized cjHtt-1 siRNA were as follows:

Sense: 5′-GCCUUUGAGUCCCUCAAGUUU-3′
Antisense: 5′-ACUUGAGGGACUCAAAGGCUU-3′

2.7. Sequence data and computational analyses

The *Htt* sequnece data derived from various species were as follows [GenBank accession number]: human (*Homo sapiens*) [NM_002111]; chimp (*Pan troglodytes*) [XM_517080]; rhesus macaque (*Macaca mulatta*) [XM_001086119]; canine (*Canis lupus familiaris*) [XM_536221]; bovine (*Bos taurus*) [XM_866758]; wild boar (*Sus scrofa*) [NM_213964]; mouse (*Mus musclus*) [NM_010414]; rat (*Rattus norvegicus*) [XM_573634]; chicken (*Gallus gallus*) [XM_420822]. Although the rhesus macaque Htt sequence [XM_001086119] contains 20 undetermined nuclotides at positons 4932–4951 followed by 6 suspensive amino acid sequences, the sequence was used and examined together with the other sequneces in this study.

Sequence homology analysis of either nucleotide or amino acid sequences was carried out by means of the GENETYX software (Software Development Co., Ltd., Tokyo, Japan), where all the parameters were set at default. For identification of the HEAT repeats in the Cj-Htt protein sequences, the REP program (http://www.embl-heidelberg.de/~andrade/papers/rep/search.html) developed by Andrade et al. was used.

3. Results and discussion

3.1. Isolation and characterization of the common marmoset Htt gene

To isolate and identify the common marmoset *Htt* (*Cj-Htt*) gene and/or gene products, we focused on conserved regions in the *Htt* gene and isolate cDNA clone of the *Cj-Htt* transcript. Highly homologous regions (sequences) between the human and mouse *Htt* genes, whose corresponding regions in the *Cj-Htt* gene were also expected to remain conserved, were selected, and PCR primers were designed for such regions. We add that such conserved regions are also detectable by BLAST search with the human *Htt* as a query on the Trace archive of the Cj-database in NCBI. RT-PCR with the designed primers and total RNA extracted from common marmoset brain tissue and established cell lines was carried out, and an approximately 9.4 kb long PCR product, which was expected to contain the full-length open reading frame (ORF) of *Cj-Htt*, was obtained (Fig. 1). The PCR product was subjected to sequence determination and then compared with various species' *Htt* genes. From the results, it was clear that the PCR product, which is 9396 nucleotides in length, was derived from the common marmoset *Htt* gene which encodes a predicted 3131 amino acid long Cj-Htt polypeptide (the sequence accession number in GenBank is AB443866). Sequence homologies in the *Htt* gene among various species are indicated in Table 1. From the data, it appears that both the nucleotide and predicted amino acid sequences of the *Cj-Htt*

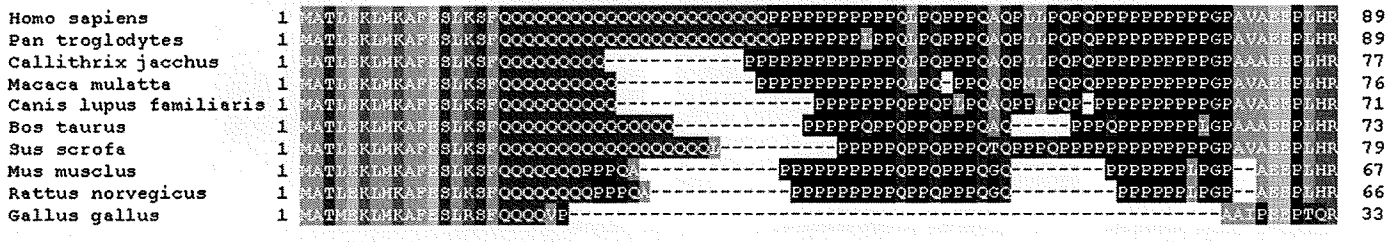

Fig. 2. Alignment of amino acid sequences in the Htt exon 1 and its corresponding regions. Sequence data were aligned based on the human Htt exon 1 (top line). Amino acid residues are color-coded based on the biochemical properties of the residues: hydrophobic amino acids in orange, polar amino acids with uncharged R groups in green, acidic amino acids in pink, basic amino acids in light blue, and special amino acids in dark blue.

Table 2
Alignment of HEAT repeats

Repeat*	Species**	AA position		Fragment†	Score	E-value
		From	To			
HEAT_AAA	Hs - Htt	124	162	QKLLGIAMELFLLCSDDAESDVRMVADECLNKVIKALMD	1510	1.26E-06
	Cj - Htt	112	150	QKLLGIAMELLLLCSDDAESDVRMVADECLNKVIKALMD	1590	5.48E-07
HEAT_AAA	Hs - Htt	205	243	RPYLVNLLPCLTRTSKRPEESVQETLAAAVPKIMASFGN	1990	1.03E-04
	Cj - Htt	193	231	RPYLVNLLPCLTRTSKRPEESVQETLAAAVPKIMASFGN	1990	2.37E-08
HEAT_AAA	Hs - Htt	247	285	DNEIKVLLKAFIANLKSSSPTIRRTAAGSAVSICQHSRR	1590	5.48E-07
	Cj - Htt	235	273	DNEIKILLKAFIANLKSSSPTIRRTAAGSAVSICQHSRR	1590	1.97E-06
HEAT_AAA	Hs - Htt	317	355	LLTLRYLVPLLQQQVKDTSLKGSFGVTRKEMEVSPSAEQ	1620	1.11E-06
	Cj - Htt	305	343	LLTLRYLVPLLHQQVKDTSLKGSFGVTRKEMEVSPSAEQ	1570	1.46E-07
HEAT_ADB	Hs - Htt					
	Cj - Htt	734	771	YPEEQYVSDILNYIDHGDPQVRGATAILCGTLVCSILS	1450	3.29E-07
HEAT_AAA	Hs - Htt	803	841	TFSLADCIPLLRKTLKDESSVTCKLACTAVRNCVMSLCS	1500	5.78E-07
	Cj - Htt	791	829	TFSLADCVPLLRKTLKDESSVTCKLACTAVRHCVMSLCS	1449	2.90E-06
HEAT_AAA	Hs - Htt	904	942	KLQERVLNNVVIHLLGDEDPRVRHVAAASLIRLVPKLFY	1930	6.69E-08
	Cj - Htt	892	930	TLQERVLTSVVIHLLGDEDPRVRHVAAASLIRLVPKLFY	2150	2.51E-05
HEAT_AAA	Hs - Htt	984	1025	RIYRGYNLLPSITDVTMENNLSRVIAAVSHELITSTTRALTF	1370	9.05E-06
	Cj - Htt	972	1013	RIYRGYNLLPSIIDVTMENNLSRVIAAVSHELITSTTRALTF	1410	2.71E-06
HEAT_AAA	Hs - Htt	1425	1463	RLFEPLVIKALKQYTTTTCVQLQKQVLDLLAQLVQLRVN	1370	5.62E-06
	Cj - Htt	1413	1451	RLFEPLVIKALKQYTTTTSVQLQKQVLDLLAQLVQLRVN	1580	3.20E-07
HEAT_AAA	Hs - Htt	2798	2836	DDTAKQLIPVISDYLLSNLKGIAHCVNIHSQQHVLVMCA	1430	3.51E-06
	Cj - Htt	2785	2823	DDTAKQLIPVISDYLLSSLKGLAHCVNTHSQQHVLVMCA	1430	3.29E-06

* HEAT_AAA and HEAT_ADB indicate subsets of HEAT repeats representing PP2A and adaptin families, respectively.
** Hs-Htt and Cj-Htt indicate the human and common marmoset Htt proteins, respectively.
†Amino acids which are different from the sequence of Hs-Htt are indicated in red.

cDNA have significant sequence homology to that of other species' *Htt* genes. In addition, it should be noted that *Htt* sequences between the human and common marmoset (colored in yellow in Table 1) appear to be particularly conserved as compared with sequence conservation within non-primate *Htt* genes, suggesting that the *Htt* gene is highly conserved in primates.

Fig. 2 shows the alignment of amino acid sequences encoded by *Htt* exon 1 and its corresponding region in various species. From the alignment, *Cj-Htt* appears to possess a short polyglutamine tract of nine glutamines compared with that of the human and chimpanzee *Htt* genes; but other than the polyglutamine tract, the exon 1 corresponding region in *Cj-Htt* exhibits high sequence homology to the human *Htt* exon 1. It is also interesting that polyproline region adjacent to the polyglutamine tract has differences between primates and non-primates: amino acid substitutions and deletions are observed, and the lack of the polyproline region in the *Gallus gallus Htt* exon 1 is particularly remarkable. These differences may influence folding and aggregation of the Htt protein, and might represent adaptive evolution of *Htt* to each species. The difference in the exon 1 among various species may provide us with a hint for understanding the expansion of the polyglutamine tract in Huntington's disease in human.

Other than the exon 1 region, we also investigated the HEAT repeats possessing tandem arrayed bihelical structure, which appear to wrap around target substrates (Andrade and Bork, 1995; Neuwald and Hirano, 2000), and found that the HEAT repeats are also conserved in the Cj-Htt protein (Table 2). In addition, it may be interesting that HEAT_ADB, a subset of HEAT repeats representing adaptin family, is present in Cj-Htt, but not in Hs-Htt.

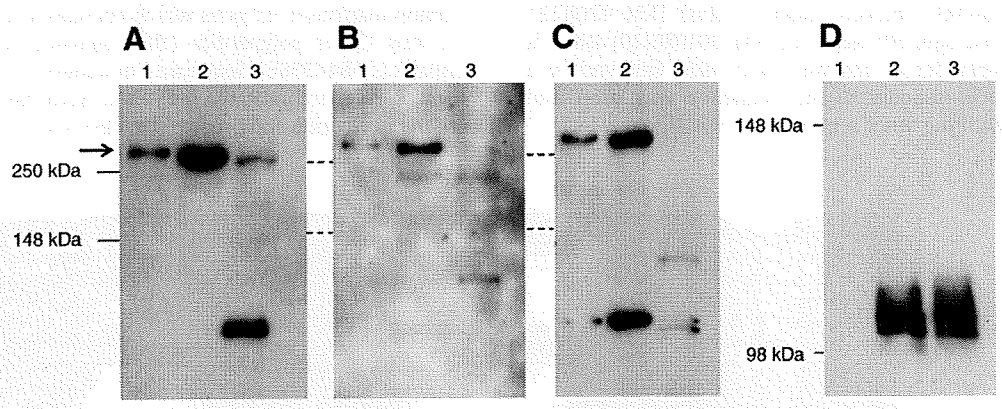

Fig. 3. Assessment of anti-human Htt antibodies against the common marmoset Htt polypeptide. Cell lysate derived from the common marmoset cell line (HSCj-110) (lane 1), brain tissue (lane 2), and mouse brain tissue as a control (lane 3) was examined by Western blotting with anti-human Htt antibodies. Tested antibodies were as follows: (A) MAB2166 (Chemicon), (B) MAB2170 (Chemicon), and (C) ab7666 (Abcam). Arrow indicates the signals of Htt proteins. The same results as those of HSCj-110 were also obtained when HSCj-002 and-009 were used (data not shown). After detection of signals, blotted membranes were subjected to antibody removal and then incubated with anti-APP antibody [MAB348 (Chemicon)] (D) followed by the same procedure as in the anti-human Htt antibodies described above.

3.2. Detection of Cj-Htt gene products

It is important to be able to properly detect the *Cj-Htt* gene and its gene products. Since the nucleotide and predicted amino acid sequences of the *Cj-Htt* cDNA showed significantly high sequence homologies to those of the human *Htt* gene, we tested whether commercially-available TaqMan probe and antibodies against human *Htt* gene products (mRNA and protein) were also able to detect *Cj-Htt* gene products. As a result, the TaqMan probe (Fig. 5A) appears to be able to detect *Cj-Htt* mRNA. In addition, newly designed PCR primers, which are perfectly matched to *Cj-Htt*, also appear to be able to detect *Cj-Htt* mRNA (Fig. 5B).

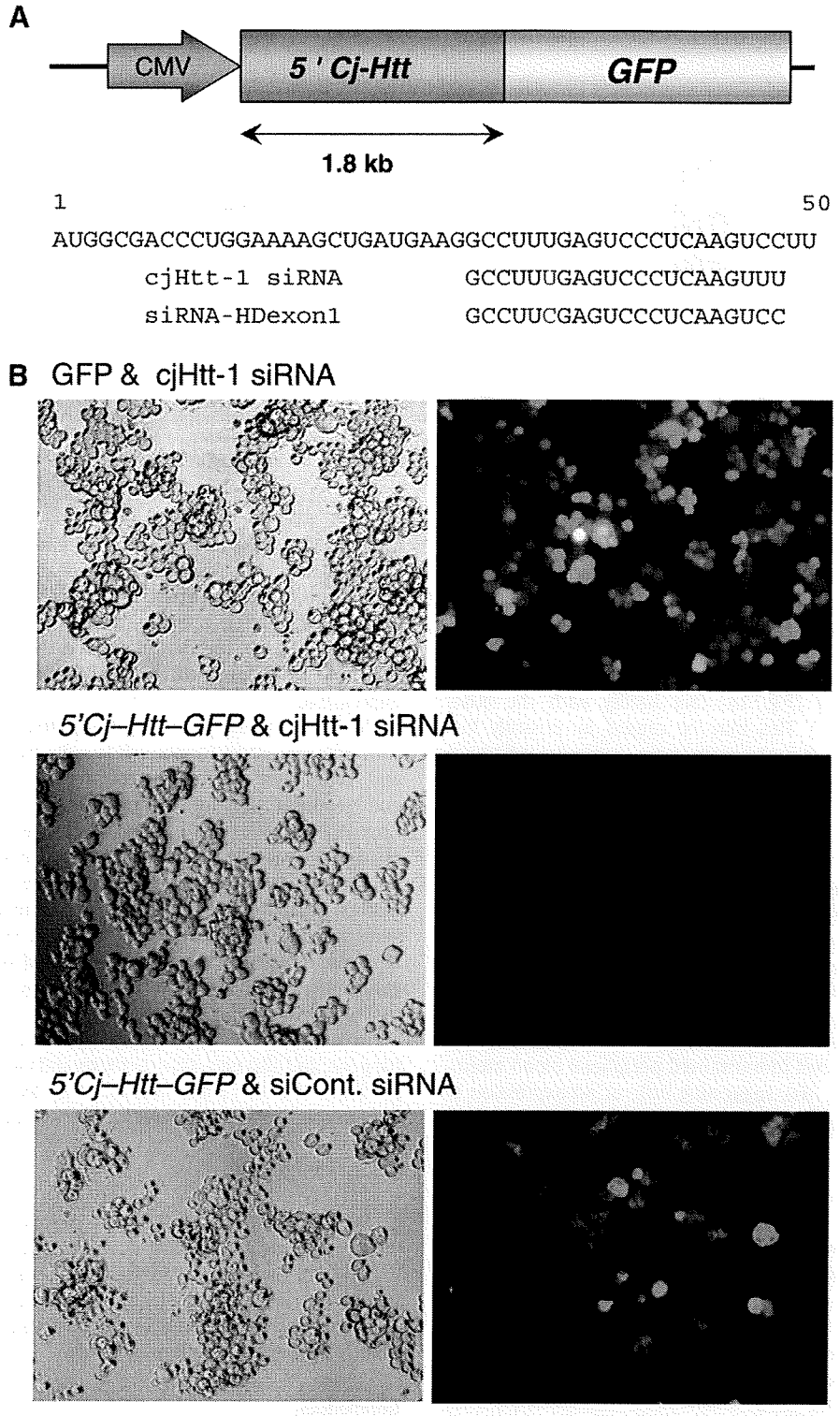

Fig. 4. Gene silencing against the 5′*Cj-Htt-GFP* fusion gene. (A) Schematic drawing of the 5′*Cj-Htt-GFP* fusion gene and designed cjHtt-1 siRNA. The fusion gene is composed of the 5′ terminal region of the Cj-Htt ORF and GFP, and driven by the Human cytomegalovirus promoter. The *Cj-Htt* sequence from the first ATG to position 50 is shown together with sequences of cjHtt-1 siRNA and siRNA-HDexon1 targeting human *Htt*. A variant nucleotide between the siRNAs is indicated in red. (B) Effect of cjHtt-1 siRNA on gene silencing. Reporter genes [5′*Cj-Htt-GFP* or *GFP* (empty reporter)] and siRNAs [cjHtt-1 or siCont (non-silencing siRNA)] were introduced into mouse neuroblastoma Neuro2a (N2a) cells. Two days after transfection, the cells were examined by a fluorescent microscope. Left (differential interference contrast) and right (fluorescence image) panels are identical in the visual field.

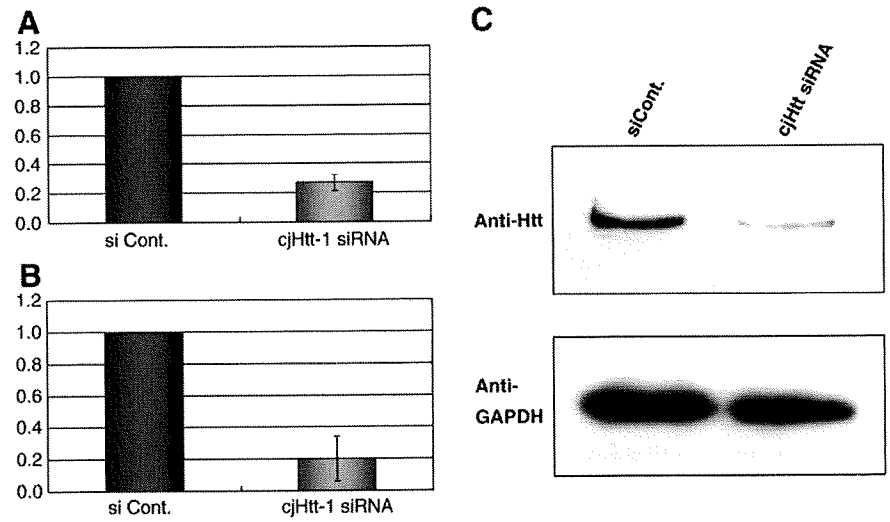

Fig. 5. Inhibition of expression of endogenous *Cj-Htt* by RNAi. The cjHtt-1 siRNA was introduced into HSCj-009 cells by means of electroporation. Two days after transfection, total RNA and cell lysate were prepared and examined by RT-real time PCR and Western blotting, respectively. Total RNA was subjected to cDNA synthesis as in Fig. 1. The resultant cDNA was examined by real time PCR with a TaqMan probe for the human *Htt* gene (A) and newly designed PCR primers [cjHtt(1139)-F and cjHtt(1254)-R] (B). The expression of *Gapdh* as a control was also examined using Perfect Real Time Primers for the human *GAPDH* gene (TAKARA BIO). The expression level of *Cj-Htt* was normalized against that of *Gapdh*, and the ratios of *Cj-Htt* expression level in the presence of cjHtt-1 siRNA were normalized against the ratio obtained in the presence of the siControl siRNA (siCont.). Data are means of at least three independent determinations. Error bars represent standard deviations. (C) Western blot. Cell lysate was examined by Western blotting with anti-human Htt antibody (MAB2166; Chemicon) as in Fig. 3. After detection of signals, the expression of GAPDH as a control was also examined by anti-GAPDH antibody (AM4300; Ambion).

Western blot analyses indicate that a polypeptide of approximately 350 kDa, which is almost the same as the molecular weight estimated from the amino acid sequence (346 kDa) in the *Cj-Htt* cDNA, can be detected in the common marmoset specimens by the antibodies tested, suggesting that the Cj-Htt protein is detectable with the antibodies (Figs. 3A–C). The 350 kDa mouse Htt protein was detected by the MAB2166 antibody (Fig. 3A), but hardly with the other antibodies (Figs. 3B and C). This may be caused by possibly low expression level of mouse Htt in the brain tissue, and/or by difference in the epitope sequences between the common marmoset and mouse Htt proteins. Other than the 350 kDa band, a few bands migrated faster than the 350 kDa band were also observed. They may be degradation products of the Htt protein, and different cells and/or species might have different degradation of the protein. To clarify these, further studies need to be carried out.

In addition to the Htt protein, we also examined the expression of amyloid precursor protein (App) with the 22C11 antibody, which can recognize the same amino acid sequence at positions 66–81 of either the human or mouse App. As a result, the App signal was able to be detected in either the common marmoset or mouse brain tissue, but not in the common marmoset immortalized peripheral blood mononuclear cells (PBMCs) (Fig. 3D), suggesting little or no expression of App in PBMCs and availability of the antibody for detection of the Cj-App protein.

3.3. Gene silencing against the Cj-Htt gene

To verify the data presented here and tools for the detection of *Cj-Htt*, we carried out gene silencing against the expression of endogenous *Cj-Htt* by means of RNA interference (RNAi), and assessed the knockdown potency of designed siRNA targeting *Cj-Htt* using the tools evaluated above. Based on a previous study where a competent siRNA duplex, siRNA-HDexon 1, conferring strong inhibition against the expression of the human *Htt* gene was used (Liu et al., 2003), we chemically synthesized an siRNA duplex, cjHtt-1 siRNA, corresponding to the siRNA-HDexon 1 duplex; note that there is one nucleotide change between cjHtt-1 siRNA and siRNA-HDexon 1 (Fig. 4A).

To examine the effect of the siRNA duplex on gene silencing, we constructed a reporter plasmid carrying the 5′ terminal region of *Cj-Htt* cDNA linked with the *GFP* reporter gene (the 5′*Cj-Htt-GFP* fusion gene). The reporter plasmid and the siRNA were cotransfected into mouse Neuro2a cells, and the expression of the 5′*Cj-Htt-GFP* fusion gene was examined by a fluorescent microscope. As shown in Fig. 4B, the data indicated that the cjHtt-1 siRNA duplex was able to induce strong RNAi activity against the fusion gene expression.

Next, we introduced the cjHtt-1 siRNA duplex into immortalized common marmoset mononuclear cells by means of electroporation, and two days after transfection, the expression levels of the endogenous *Cj-Htt* mRNA and protein were examined by RT-real time PCR and Western blotting, respectively. As shown in Fig. 5, the results consistently indicated that *Cj-Htt* mRNA (A and B) and protein (C) levels markedly decreased in the presence of the cjHtt-1 siRNA duplex, i.e., potent RNAi knockdown against the endogenous *Cj-Htt* gene was induced by the siRNA duplex. Finally, the data presented here also indicate that proper detection of the newly identified *Cj-Htt* gene and its products can be performed by means of the methods and tools assessed in this study.

In conclusion, we described for the first time the common marmoset *Htt* gene, and also detection methods and tools for the gene and its gene products. The data presented here may assist us in promoting a non-human primate HD model with the common marmoset.

Acknowledgments

We would like to thank Dr. R.C. Desrosiers for kindly providing HS viruses. We also thank Drs. K. Nakamura, T. Kabuta, M. Suzuki, and C. Konya for their helpful advice and discussion. Finally, we would like to thank Dr I. Kanazawa for his encouragement and helpful advice. This work was supported by research grants from the Ministry of Health, Labour and Welfare of Japan.

References

Akari, H., et al., 1996. In vitro immortalization of Old World monkey T lymphocytes with Herpesvirus saimiri: its susceptibility to infection with simian immunodeficiency viruses. Virology 218, 382–388.

Andrade, M.A., Bork, P., 1995. HEAT repeats in the Huntington's disease protein. Nat. Genet. 11, 115–116.

Deisboeck, T.S., et al., 2003. Development of a novel non-human primate model for preclinical gene vector safety studies. Determining the effects of intracerebral HSV-1 inoculation in the common marmoset: a comparative study. Gene Ther. 10, 1225–1233.
Doods, H., et al., 2000. Pharmacological profile of BIBN4096BS, the first selective small molecule CGRP antagonist. Br. J. Pharmacol. 129, 420–423.
Gilliam, T.C., et al., 1987. A DNA segment encoding two genes very tightly linked to Huntington's disease. Science 238, 950–952.
Gusella, J.F., et al., 1983. A polymorphic DNA marker genetically linked to Huntington's disease. Nature 306, 234–238.
Huntington's-Disease, C.R.G.o., The Huntington's Disease Collaborative Research Group, 1993. A novel gene containing a trinucleotide repeat that is expanded and unstable on Huntington's disease chromosomes. Cell 72, 971–983.
Kazemi-Esfarjani, P., Benzer, S., 2000. Genetic suppression of polyglutamine toxicity in Drosophila. Science 287, 1837–1840.
Kendall, A.L., Rayment, F.D., Torres, E.M., Baker, H.F., Ridley, R.M., Dunnett, S.B., 1998. Functional integration of striatal allografts in a primate model of Huntington's disease. Nat. Med. 4, 727–729.
Liu, W., Goto, J., Wang, Y., Murata, M., Wada, K., Kanazawa, I., 2003. Specific inhibition of Huntington's disease gene expression by siRNAs in cultured cells. Proc. Jpn. Acad. 79, 293–298.
Lunkes, A., Mandel, J.L., 1998. A cellular model that recapitulates major pathogenic steps of Huntington's disease. Hum. Mol. Genet. 7, 1355–1361.
Mangiarini, L., et al., 1996. Exon 1 of the HD gene with an expanded CAG repeat is sufficient to cause a progressive neurological phenotype in transgenic mice. Cell 87, 493–506.
Neuwald, A.F., Hirano, T., 2000. HEAT repeats associated with condensins, cohesins, and other complexes involved in chromosome-related functions. Genome Res. 10, 1445–1452.
Palfi, S., et al., 2007. Expression of mutated huntingtin fragment in the putamen is sufficient to produce abnormal movement in non-human primates. Mol. Ther. 15, 1444–1451.
Sakai, T., Hohjoh, H., 2006. Gene silencing analyses against amyloid precursor protein (APP) gene family by RNA interference. Cell Biol. Int. 30, 952–956.
t'Hart, B.A., Vervoordeldonk, M., Heeney, J.L., Tak, P.P., 2003. Gene therapy in nonhuman primate models of human autoimmune disease. Gene Ther. 10, 890–901.
von Horsten, S., et al., 2003. Transgenic rat model of Huntington's disease. Hum. Mol. Genet. 12, 617–624.
Walker, F.O., 2007. Huntington's disease. Lancet 369, 218–228.
Yang, S.H., et al., 2008. Towards a transgenic model of Huntington's disease in a non-human primate. Nature 453, 921–924.

Retrovirology

BioMed Central

Research

Open Access

MDM2 is a novel E3 ligase for HIV-1 Vif

Taisuke Izumi[1], Akifumi Takaori-Kondo*[1], Kotaro Shirakawa[1,2], Hiroaki Higashitsuji[3], Katsuhiko Itoh[3], Katsuhiro Io[1], Masashi Matsui[1], Kazuhiro Iwai[4,5], Hiroshi Kondoh[6], Toshihiro Sato[7], Mitsunori Tomonaga[7], Satoru Ikeda[7], Hirofumi Akari[8], Yoshio Koyanagi[9], Jun Fujita[3] and Takashi Uchiyama[1]

Address: [1]Department of Hematology and Oncology, Graduate School of Medicine, Kyoto University, 54 Shogoin-Kawaracho, Sakyo-ku, Kyoto 606-8507, Japan, [2]Japanese Foundation for AIDS Prevention, 1-3-12 Misaki-cho, Chiyoda-ku, Tokyo 101-0061, Japan, [3]Department of Clinical Molecular Biology, Graduate School of Medicine, Kyoto University, 54 Shogoin-Kawaracho, Sakyo-ku, Kyoto 606-8507, Japan, [4]Department of Molecular Cell Biology, Graduate School of Medicine, Osaka City University, 1-4-3 Asahi-machi, Abeno-ku, Osaka 545-8585, Japan, [5]CREST, Japan Science Technology Corporation, Kawaguchi, Saitama 332-0012, Japan, [6]Department of Geriatric Medicine, Graduate School of Medicine, Kyoto University, 54 Shogoin-Kawaracho, Sakyo-ku, Kyoto 606-8507, Japan, [7]Central Pharmaceutical Research Institute, Japan Tobacco Inc., 1-1 Murasaki-cho, Takatsuki, Osaka 569-1125, Japan, [8]Laboratory of Disease Control, Tukuba Primate Research Center, National Institute of Biomedical Innovation, Hachimandai-1, Tsukuba, Ibaraki 305-0843, Japan and [9]Laboratory of Viral Pathgenesis, Institute for Virus Research, Kyoto University, 53 Shogoin-Kawaracho, Sakyo-ku, Kyoto 606-8507, Japan

Email: Taisuke Izumi - izumi.t@aw3.ecs.kyoto-u.ac.jp; Akifumi Takaori-Kondo* - atakaori@kuhp.kyoto-u.ac.jp; Kotaro Shirakawa - kotash@kuhp.kyoto-u.ac.jp; Hiroaki Higashitsuji - hhigashi@virus.kyoto-u.ac.jp; Katsuhiko Itoh - katsu@virus.kyoto-u.ac.jp; Katsuhiro Io - katsu829@kuhp.kyoto-u.ac.jp; Masashi Matsui - mmatsui@kuhp.kyoto-u.ac.jp; Kazuhiro Iwai - kiwai@cellbio.med.osaka-u.ac.jp; Hiroshi Kondoh - hkondoh@kuhp.kyoto-u.ac.jp; Toshihiro Sato - toshihiro.sato@ims.jti.co.jp; Mitsunori Tomonaga - mitsunori.tomonaga@ims.jti.co.jp; Satoru Ikeda - satoru.ikeda@ims.jti.co.jp; Hirofumi Akari - akari@nibio.go.jp; Yoshio Koyanagi - ykoyanag@virus.kyoto-u.ac.jp; Jun Fujita - jfujita@virus.kyoto-u.ac.jp; Takashi Uchiyama - uchiyata@kuhp.kyoto-u.ac.jp

* Corresponding author

Published: 7 January 2009

Retrovirology 2009, **6**:1 doi:10.1186/1742-4690-6-1

Received: 16 September 2008
Accepted: 7 January 2009

This article is available from: http://www.retrovirology.com/content/6/1/1

Abstract

The human immunodeficiency virus type 1 (HIV-1) Vif plays a crucial role in the viral life cycle by antagonizing a host restriction factor APOBEC3G (A3G). Vif interacts with A3G and induces its polyubiquitination and subsequent degradation via the formation of active ubiquitin ligase (E3) complex with Cullin5-ElonginB/C. Although Vif itself is also ubiquitinated and degraded rapidly in infected cells, precise roles and mechanisms of Vif ubiquitination are largely unknown. Here we report that MDM2, known as an E3 ligase for p53, is a novel E3 ligase for Vif and induces polyubiquitination and degradation of Vif. We also show the mechanisms by which MDM2 only targets Vif, but not A3G that binds to Vif. MDM2 reduces cellular Vif levels and reversely increases A3G levels, because the interaction between MDM2 and Vif precludes A3G from binding to Vif. Furthermore, we demonstrate that MDM2 negatively regulates HIV-1 replication in non-permissive target cells through Vif degradation. These data suggest that MDM2 is a regulator of HIV-1 replication and might be a novel therapeutic target for anti-HIV-1 drug.

Background

Host restriction factors protect hosts from viruses, whereas viruses evade these proteins to replicate more efficiently in host cells. The interplay between the host restriction factors and viral proteins is therefore very important for regulating viral replication [1,2]. A3G (Apolipoprotein B mRNA editing enzyme, catalytic polypeptide-like 3G) is a newly identified anti-HIV-1 host factor [3], which belongs to the APOBEC superfamily of cytidine deaminases, consisting of APOBEC1, APOBEC2, AID (activation-induced cytidine deaminase), APOBEC3(A-H), and APOBEC4 [4]. A3G is incorporated into HIV-1 virions and inhibits HIV-1 replication by inducing G-to-A hypermutation in viral cDNA during reverse transcription [5-8]. HIV-1 Vif counteracts A3G by targeting it for proteasomal degradation, thus supporting HIV-1 replication in non-permissive target cells [9-11]. Vif forms a ubiquitin ligase (E3) complex with Cullin5 (Cul5), Elongin B, and Elongin C and functions as a substrate recognition subunit of this complex to induce ubiquitination and subsequent degradation of A3G [12,13]. Vif also counteracts several APOBEC3 proteins including APOBEC3F (A3F) [14,15]. These observations reconcile the long-standing mystery of why Vif function is necessary for HIV-1 to infect non-permissive cells. On the other hand, it has been shown that intracellular levels of Vif are maintained relatively low by ubiquitination in virus-producing cells [16-18]. Although several groups have reported E3 ligases important for Vif ubiquitination [17,18], the precise roles and mechanisms of Vif ubiquitination remain unclear. Here we demonstrate that MDM2 is a novel E3 ligase for Vif and that it induces ubiquitination and degradation of Vif, thereby regulating HIV-1 replication.

Results

MDM2 downregulates cellular Vif levels by inducing its degradation in a proteasome-dependent manner

To investigate the biological roles and molecular mechanisms of Vif ubiquitination, we tried to identify a novel E3 ligase that may be involved in the ubiquitination of Vif. During a search for Vif-interacting proteins in the HIV, Human Protein Interaction Database of National Institute for Allergy & Infectious Diseases http://www.ncbi.nlm.nih.gov/RefSeq/HIVInteractions/, we were struck by a protein called Gankyrin (proteasome 26S subunit, non-ATPase, 10 (PSMD10)). We first examined the biological effects of Gankyrin, but could not detect a downregulation of Vif (data not shown). As we previously reported that Gankyrin itself doesn't have an enzymatic activity and that it rather enhances the E3 ligase activity of MDM2 on p53 ubiquitination and degradation as a co-factor [19], we tested the possibility that MDM2 plays an important role in Vif ubiquitination as a novel E3 ligase. We examined the effect of several E3 ligases including MDM2 (a RING finger type E3 that mediates p53 ubiquitination and degradation [20]), Cul5 (another RING finger type E3 that forms a complex with Vif and is reported to induce Vif ubiquitination [17,21]), and Parkin (another RING finger type E3) on cellular Vif levels (Fig. 1A). HEK293T cells were transfected with a subgenomic expression vector pNL-A1 that expressed all HIV-1 proteins except for *gag* and *pol* products [22], together with the expression plasmids for these E3 ligases. We found that the ectopic expression of MDM2 downregulated the cellular levels of Vif as well as p53 in transfected cells in a dose-dependent manner (Fig. 1A, lanes 8–10), whereas Parkin and Cul5 did not affect their cellular levels (lanes 2–4 and 5–7, respectively), even though the latter proteins were expressed more than MDM2. Our results are discrepant with previous reports that demonstrated Cul5 induced Vif ubiquitination and degradation [17,23]. We assume that overexpression of Cul5 alone is insufficient to induce Vif degradation, because other E3 components are not overexpressed. Ectopic expression of MDM2 did not affect cellular levels of another viral protein such as Nef, suggesting that MDM2 specifically downregulated Vif levels; this result also excluded the possibility that MDM2 affected the transcriptional activity of the HIV-1 LTR.

Because it is well known that MDM2 regulates p53 levels by modulating its protein stability, we next examined the protein stability of Vif with the ectopic expression of MDM2. HEK293T cells were transfected with pNL-A1 with or without a MDM2 expression vector and treated with cycloheximide 21 hrs after transfection. After cycloheximide treatment, cellular levels of Vif decreased by 60% in MDM2-transfected cells and by 20% in control cells, respectively (Fig. 1B &1C), indicating that Vif decayed much faster when MDM2 was overexpressed. The stability profile of Vif protein was similar to that of p53 (Fig. 1B). However, in our hands, the half-life of Vif protein was longer than those shown in previous studies from several laboratories. We interpret that this difference is attributable to divergent methods used in the studies which employed radioisotopes or cycloheximide. Thus, our findings suggest that MDM2 affects the stability of Vif protein similar to its effect on p53. We also examined the stability of Vif in MDM2-/- MEF cells. Vif decayed much faster in p53-/- MEF cells than in p53-/-MDM2-/- double knock-out (DKO) MEF cells (Additional file 1), suggesting that endogenous MDM2 can also influence the stability of Vif. We then tested a RING finger domain-deleted MDM2 mutant, ΔRF, which is inactive for the ubiquitination activity of MDM2 [24]. Ectopic expression of MDM2 suppressed cellular Vif levels, but the expression of ΔRF did not (Fig. 1D). This result suggests that ubiquitination of Vif by MDM2 is involved in the downregulation of cellular Vif levels. We further treated transfected cells with a proteasome inhibitor MG132 to see whether the down-

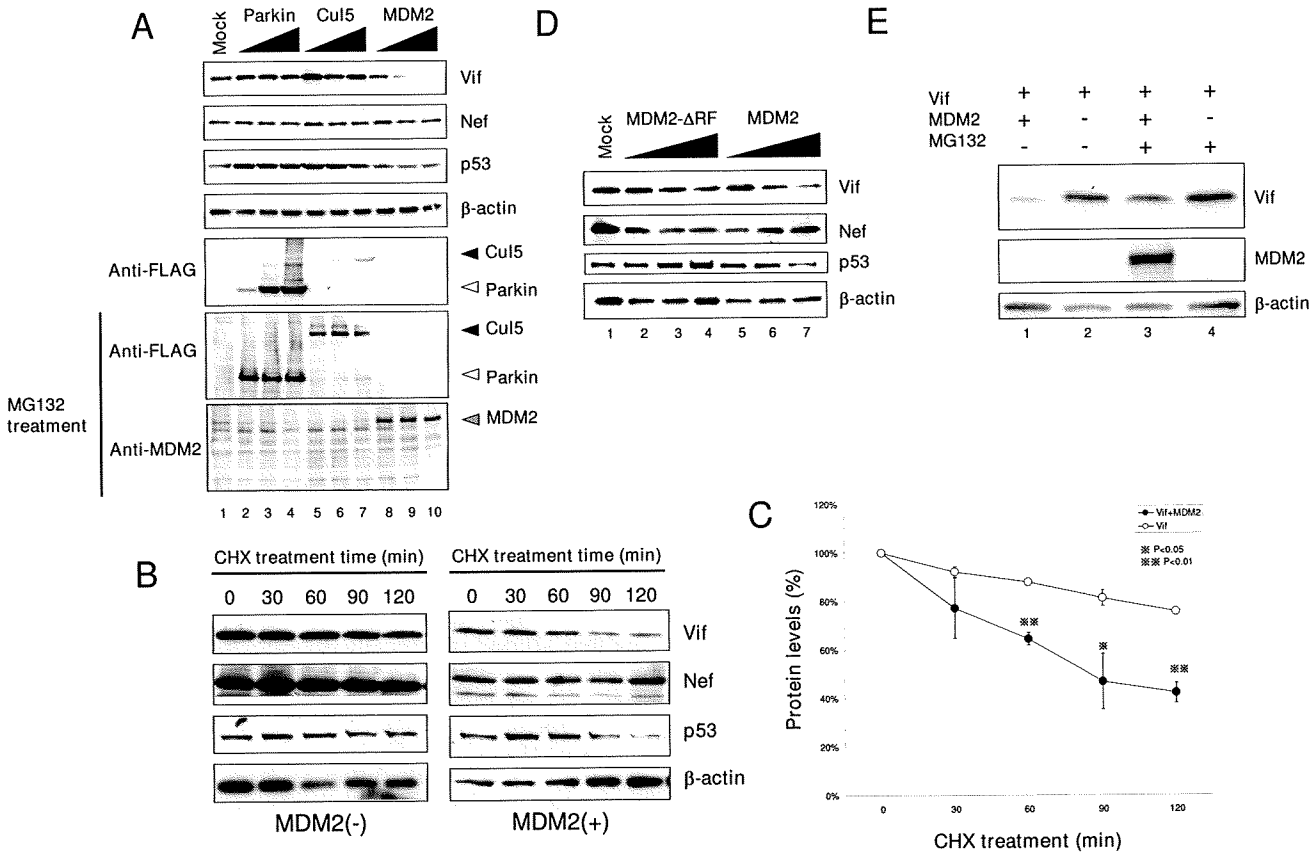

Figure 1

MDM2 downregulated cellular Vif levels in a proteasome dependent manner. (A) MDM2 reduced cellular levels of Vif as well as p53, but not that of Nef. HEK293T cells were cotransfected with expression vectors for the indicated E3 ligases and a subgenomic HIV-1 expression vector pNL-A1. Cell lysates were subjected to immunoblotting with the indicated Abs. We could not detect the expression of FLAG-MDM2 without MG132 treatment, because of a rapid degradation of MDM2. MG132 treatment enabled us to detect expression of MDM2 only with anti-MDM2 Ab, but not with anti-FLAG mAb. (B) Twenty-two hours after transfection, the cells were treated with cycloheximide (CHX)(80 μg/ml) for the indicated times, and cell lysates were subjected to immunoblotting with the indicated Abs. (C) The amounts of Vif and Nef were quantified by densitometry, and Vif protein levels were calculated using Nef protein levels as normalizing loading controls and presented as percentage values relative to that without CHX treatment set as 100%. Values are presented as averages of three independent experiments. (D) MDM2 downregulated Vif, but a ΔRF mutant did not. HEK293T cells were cotransfected with expression vectors for MDM2 and the mutant together with pNL-A1, and cell lysates were subjected to immunoblotting with the indicated Abs. (E) $p53^{-/-}MDM2^{-/-}$ DKO-MEF cells were cotransfected with expression vectors for MDM2 and Vif, and treated with 10 μM MG132 for 6 hrs, and cell lysates were subjected to immunoblotting with the indicated Abs.

regulation of Vif by MDM2 was proteasome-dependent. Treatment with MG132 clearly restored the cellular Vif level that was downregulated by MDM2 (Fig. 1E, top panel, lane 3 as compared with lane 1), supporting that the MDM2-mediated downregulation of Vif was proteasome-dependent. Taken together, we concluded that MDM2 downregulates cellular Vif level by inducing its degradation in a proteasome-dependent manner.

MDM2 specifically binds and downregulates Vif

To further investigate the molecular link between MDM2 and Vif, we next examined the physical interaction of MDM2 with Vif. Immunoprecipitation assays showed that Vif was co-precipitated with MDM2 (Fig. 2A). Glutathione S-transferase (GST) pull-down assays showed that MDM2 was found in GST-Vif-bound, but not GST-bound, material (data not shown). Using a series of MDM2 deletion mutants, we determined that the central region of MDM2 (amino acids 168–320) was necessary for Vif binding (Fig. 2B, left panel &2C). To more precisely

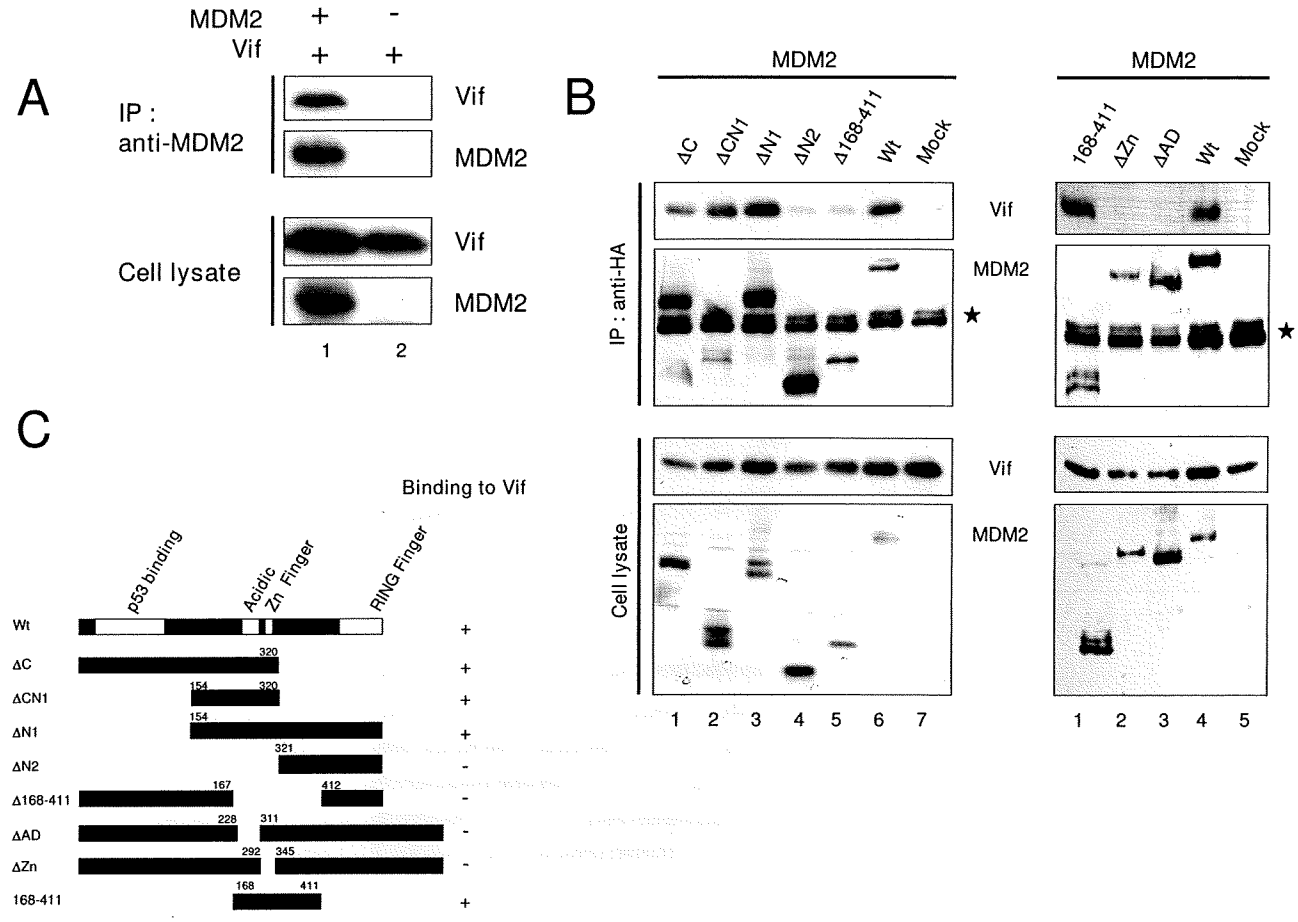

Figure 2
MDM2 bound Vif in its central domain. (A) Immunoprecipitation assays revealed the interaction of MDM2 with Vif *in vivo*. HEK293T cells were cotransfected with expression vectors for MDM2 and Vif and treated with MG132 for 6 hrs prior to harvest. Cell lysates were immunoprecipitated with anti-MDM2 mAb followed by immunoblotting with the indicated Abs (upper two panels). Cell lysates were also subjected to immunoblotting with the indicated Abs (lower two panels). (B) The interaction domain of MDM2 with Vif. HEK293T cells were cotransfected with expression vectors for HA-tagged MDM2 wild type (Wt) and mutants together with pNL-A1, and cell lysates were immunoprecipitated with anti-HA mAb followed by immunoblotting with the indicated Abs. Asterisk indicates immunoglobulin heavy chains from thenimmunoprecipitation. (C) Schematics of MDM2 mutants binding to Vif are shown.

determine a Vif-binding domain, we further tested mutants deleted in a Zn Finger domain (ΔZn) or in an acidic domain (ΔAD). Neither mutant could bind Vif, whereas the mutant containing amino acids 168–411 was able to bind Vif, suggesting that both domains are necessary and that the central domain is sufficient for Vif binding (Fig. 2B, right panel &2C). Additionally, using a series of Vif deletion mutants, we also found that the N-terminal region of Vif (amino acids 4–22) is needed for MDM2 binding (Fig. 3A &3C). Furthermore, we examined the MDM2-mediated downregulation of Vif mutants. MDM2 was able to efficiently downregulate cellular levels of the MDM2-binding Vif mutants but not that of an MDM2-non binding mutant, Δ4–45 (Fig. 3B). Collectively, these results indicated that the Vif-MDM2 interaction is required for MDM2-mediated downregulation of Vif (Fig. 3C).

MDM2 induces ubiqutination of Vif

Since we found that MDM2 bound Vif and promoted its degradation via a proteasomal pathway, we next examined whether MDM2 is involved in the polyubiquitination of Vif. *In vitro* ubiquitination assays revealed that bacterially expressed GST-MDM2 was able to induce the

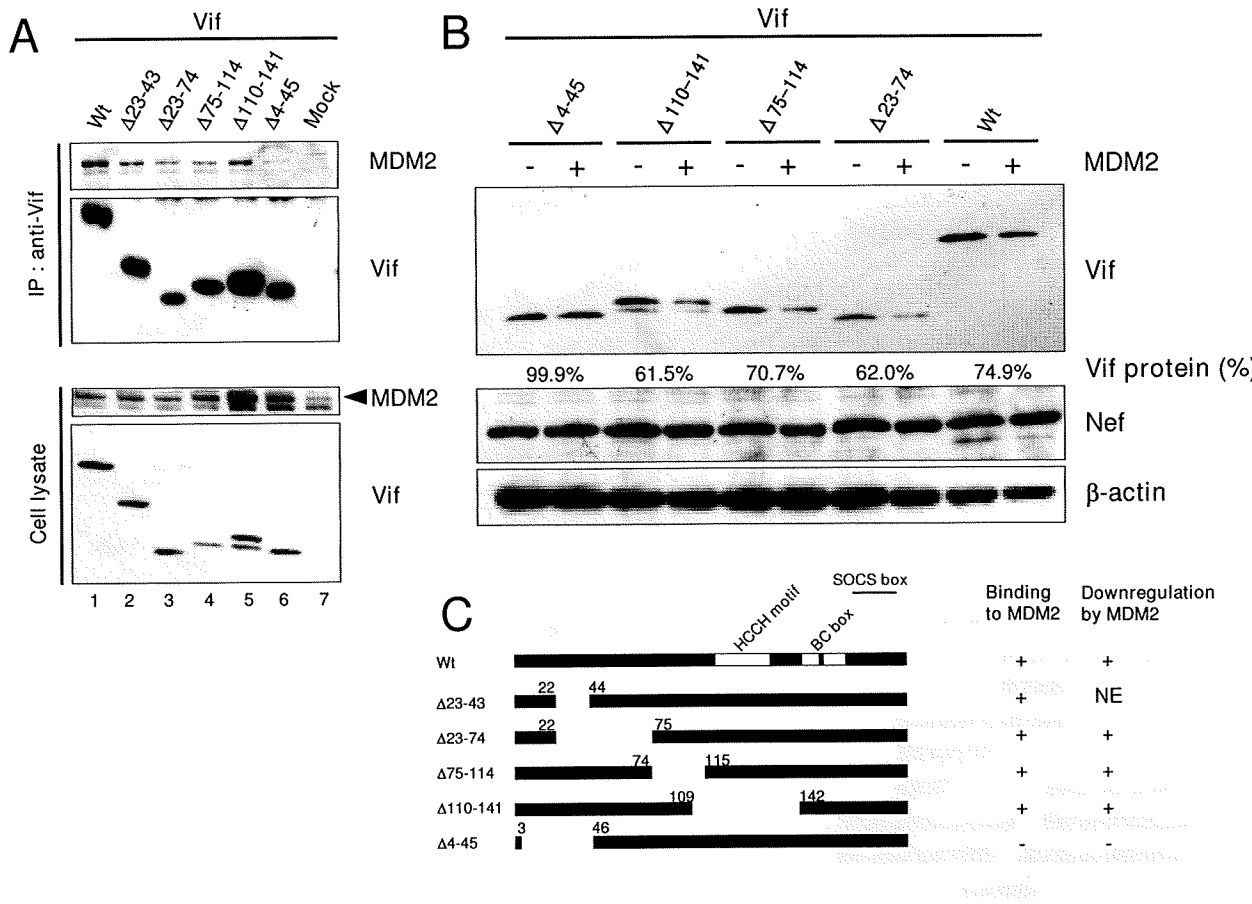

Figure 3
MDM2 specifically bound and downregulated Vif. (A) The interaction domain of Vif with MDM2. HEK293T cells were cotransfected with expression vectors for Vif and mutants together with pCMV/HA-MDM2, and cell lysates were immunoprecipitated with anti-Vif mAb followed by immunoblotting with the indicated Abs. Arrowhead indicates MDM2. (B) The downregulation of Vif protein by MDM2. HEK293T cells were cotransfected with expression vectors for Vif and mutants with or without pCMV/HA-MDM2, and cell lysates were subjected to immunoblotting with the indicated Abs. The amounts of Vif were quantified by densitometry and shown as the protein ratio relative to that without expression of MDM2. (C) Schematics of Vif mutants bound by and downregulated by MDM2. NE: not examined.

polyubiquitination of purified GST-Vif protein *in vitro* (Fig. 4A). The ubiquitination of Vif by MDM2 was specific, as the omission of ubiqutin, E1, E2, or MDM2 prevented Vif-ubiquitination as shown in our previous experiments [13]. We also performed *in vitro* ubiquitination assays using immunopurified MDM2 and Cul5. Immunopurified MDM2 was able to induce ubiquitination of Vif *in vitro* to the same extent as Cul5 (Additional file 2, part A), while it could not ubiquitinate the N-terminal Vif deletion mutant Δ22 that was defective for binding MDM2 (Additional file 2, part B). These findings suggest that the interaction with MDM2 is important for Vif ubiquitination. We performed *in vivo* ubiquitination assays to further investigate the importance of MDM2 in Vif ubiquitination. Lysates of cells co-expressing Vif, either with an MDM2 wild type (Wt) or a ΔRF mutant, and His-tagged Ubiquitin (His-Ub) were analyzed for the presence of ubiquitinated Vif conjugates (Fig. 4B). Unfortunately, we detected a Vif band that non-specifically bound to Ni-NTA agarose (arrowhead) due to its nature as a sticky protein. Overexpression of MDM2 induced a ladder detected by anti-Vif Ab, even in the absence of His-Ub (lane 2), suggesting that this ladder represented Vif protein polyubiquitinated with endogenous Ub (arrows with asterisk). Furthermore, in the presence of His-Ub, we detected a doublet of ladder which presumably represented Vif protein polyubiquitinated with endogenous and His-tagged Ub (arrows with asterisk and arrows, respectively). We also obtained similar results using a UbiQapture™-Q Kit (data not shown). We thus concluded that the overexpres-